

DEVELOPMENT OF ADVANCED GPR SIMULATION  
SYSTEM

SALEM ALI AL-OTAIBI

BY

A Thesis Presented to the  
DEANSHIP OF GRADUATE STUDIES

**KING FAHD UNIVERSITY OF PETROLEUM & MINERALS**

DHAHRAN, SAUDI ARABIA

In Partial Fulfillment of the  
Requirements for the Degree of

**MASTER OF SCIENCE**

In

**ELECTRICAL ENGINEERING**

**Jan 1, 2012**

KING FAHD UNIVERSITY OF PETROLEUM AND MINERALS

DHAHRAN 31261, SAUDI ARABIA


DEANSHIP OF GRADUATE STUDIES


This thesis, written by **Salem Ali Al-Otaibi** under the direction of his thesis advisor and approved by his thesis committee, has been presented to and accepted by the Dean of Graduate Studies, in partial fulfillment of the requirements for the degree of **MASTER OF SCIENCE IN ELECTRICAL ENGINEERING**.

Thesis Committee


  
Dr. Mohammed Alsunaidi (Advisor)


  
Dr. Ahmad Yamani (Co-advisor)

  
Dr. Abdullatif Al-Shuhail (Member)

  
Dr. Ali Muqaibel (Member)

  
Dr. Sheikh Sharif Iqbal (Member)

  
Dr. Ali Al-Shaikhi  
Department Chairman

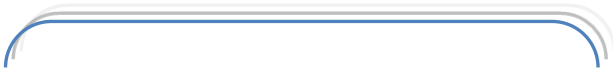
  
Dr. Salam A. Zummo  
Dean of Graduate Studies

Date

21/5/12



# DEDECATION



*Dedicated to*

*My beloved mother*

*And*

*The memory of my*

*father*



# ACKNOWLEDGEMENTS

All praise is to Allah (SWT), Lord of the Heavens and the Earths, and what they contain; most Beneficial, Most Merciful. I seek His benediction on our beloved Prophet, the best of humankind, Muhammad (SAW), his household and his companions, until the Day of Judgment. I thank Allah for His infinite bounties on me, one of which is the completion of this work; I seek His mercy and forgiveness, and indeed, I fear His wrath.

My gratitude, without reservation, goes to my mother for her endless support and prayers throughout my life. I will forever remain grateful.

I would like to convey my sincere gratitude to my thesis advisor Dr. Mohammed Abdulaziz Al-sunaidi for his support and guidance. I thank him for being available whenever I needed his assistance. It is my pleasure to work with such professor. I would like also to thank co-advisor Dr. Ahmad Yamani for his endless help and support. It is my pleasure to work with him.

Special thanks to distinguished members of my thesis committee Dr. Abdullatif Al-Shuhail, Dr. Ali Muqaibel and Dr. Sheikh Sharif Iqbal ; first, for accepting to be on my thesis committee, further, for their useful guidance, motivation, and professional contribution to my success and that of this work.

Special thanks to Robert Schwartz and Joaquin Casanova (USDA-ARS, Bushland, TX) for providing a copy of the MATLAB routine for dispersive soil data that was used in this thesis.

I acknowledge my brothers and sisters for their support; my friends for their best wishes and help; and KFUPM, for the opportunity it gave me to study and accomplish this work.

To all, I remain grateful.

# TABLE OF CONTENTS

<b>DEDECATION .....</b>	<b>iii</b>
<b>ACKNOWLEDGEMENTS .....</b>	<b>iv</b>
<b>TABLE OF CONTENTS .....</b>	<b>vi</b>
<b>LIST OF TABLES.....</b>	<b>ix</b>
<b>LIST OF FIGURES.....</b>	<b>x</b>
<b>LIST OF ACRONYMS .....</b>	<b>xiii</b>
<b>THESIS ABSTRACT (ENGLISH) .....</b>	<b>xv</b>
<b>THESIS ABSTRACT (ARABIC).....</b>	<b>xvi</b>
<b>INTRODUCTION .....</b>	<b>1</b>
1.1 Overview.....	1
1.2 Literature Review.....	3
1.3 Thesis Contribution.....	7
1.4 Thesis Organization .....	8
<b>2 GROUND PENETRATING RADAR.....</b>	<b>9</b>
2.1 Introduction.....	9
2.2 Principles of Electromagnetic Approach .....	10
2.3 Principles of GPR .....	11
2.4 GPR Wave Characteristics.....	12
2.4.1 Central Frequency .....	12

2.4.2 Wave Velocity .....	14
2.4.3 Wave Attenuation .....	15
<b>3 MATERIAL DISPERSION MODELS.....</b>	<b>16</b>
3.1 Material Models .....	16
3.2 Soil and Moisture Models.....	22
<b>4 THE FINITE DIFFERENCE TIME DOMAIN METHOD.....</b>	<b>27</b>
4.1 Introduction to the FDTD Method.....	27
4.3 The General ADE-FDTD Algorithm for Dispersive Materials .....	35
<b>5 SIMULATION RESULTS.....</b>	<b>41</b>
5.1 Algorithm Validation .....	41
5.2 Simulated Cases .....	44
5.2.1 Curve Fitting .....	44
5.2.3 First Case : Simulation of a Two-Layer System.....	50
5.2.4 Second Case: Simulation of Four Layers.....	52
5.2.5 Third Case: Simulation of Localized Wet Soil .....	56
5.2.6 Fourth Case: Simulation of Non-Metallic Pipe Leakage.....	58
<b>6 TIME-FREQUENCY ANALYSIS OF THE SIMULATED CASES.....</b>	<b>66</b>
6.1 Conventional Characteristic Features .....	66
6.2 Time-Frequency .....	67
<b>CONCLUSIONS AND RECOMMENDATIONS .....</b>	<b>73</b>
Summary and Conclusions .....	73

Recommendation for Future Research..... 74

**References 75**

**Vita 81**



# LIST OF TABLES

Table 3-1: Several dispersion types and the corresponding coefficients [50] .....	25
Table 4-1: Several electric dispersion types and the corresponding coefficients.....	39
Table 4-2: Several magnetic dispersion types and the corresponding coefficients.....	40
Table 5.1: Soil model reported in [57].....	41
Table 5.2: Multi-pole Lorentz selected parameters wet dispersive soil relations.....	45
Table 5.3: Multi-pole Debye selected parameters for the hypothetical Material.....	63

# LIST OF FIGURES

Figure 2-1: Block diagram of typical GPR system.....	11
Figure 2-2: Types of GPR resolution [38].....	13
Figure 3-1: Resonance described by the Lorentz model.....	17
Figure 3-2: Relationship between E and P in material Debye modelled dielectric.....	20
Figure 3-3: Real permittivity curves generated by the empirical model in [50].....	26
Figure 3-4: Imaginary permittivity curves generated by the empirical model in [50].	26
Figure 4-1: Yee’s spatial grid.....	29
Figure 4-2: Leapfrog temporal scheme of the FDTD method.....	31
Figure 4-3: A flowchart for the calculations involved in the general algorithm.....	40
Figure 5-1: Time profile of the signal launched by the transmitter.....	42
Figure 5-2: The frequency spectrum of the transmitted signal.....	42
Figure 5-3: The simulation domain for the validated case .....	42
Figure 5-4: Time profile of the recorded electric field (3D simulator).....	43
Figure 5-5: Time profile of the recorded electric field (2D simulator).....	43
Figure 5-6: Real and imaginary permittivity for wet soil with 40 % moisture generated by the empirical dielectric function (blue) and the corresponding 5-pole Lorentz fit (red).....	46
Figure 5-7: Real and imaginary permittivity for wet soil with 30 % moisture generated by the empirical dielectric function (blue) and the corresponding 5-pole Lorentz fit (red).....	46
Figure 5-8: Real and imaginary permittivity for wet soil with 20 % moisture generated by the empirical dielectric function (blue) and the corresponding 5-pole Lorentz fit (red).....	47
Figure 5-9: Real and imaginary permittivity for wet soil with 10 % moisture generated by the empirical dielectric function (blue) and the corresponding 5-pole Lorentz fit (red).....	47
Figure 5-10: Real and imaginary permittivity for wet soil with 10 % moisture generated by the empirical dielectric function (blue) and the corresponding 5-pole Lorentz fit (red).....	48
Figure 5-11: Time profile of the signal launched by the transmitter.....	48
Figure 5-12: The frequency spectrum of the transmitted signal.....	49
Figure 5-13: Time profile of the received signal with (blue) and without (red) consideration of the material dispersion.....	50

Figure 5-14: The simulation domain for the first case.....	51
Figure 5-15: Time profile of the received signal for different moisture levels excluding the direct path peak.....	52
Figure 5-16: The simulation domain for the second case.....	53
Figure 5-17: The simulation results in CMP configuration with 20 cm Wet Soil. ....	53
Figure 5-18: The simulation results in CMP configuration with 40 cm Wet Soil.....	54
Figure 5-19: The simulation results in CMP configuration with 60 cm Wet Soil.....	54
Figure 5-20: The simulation results from one receiver for 20, 40 and 60 cm Layer...55	
Figure 5-21: The simulation domain for the third case.....	56
Figure 5-22: The simulation results in CMP configuration for Localized 40 % Wet Soil at position 1.....	57
Figure 5-23: The simulation results in CMP configuration for Localized 40 % Wet Soil at position 2.....	57
Figure 5-24: Time profile of the received signals at different receiver locations for localized wet soil at position 1 and position 2.....	58
Figure 5-25: The simulation domain for the fourth case.....	59
Figure 5-26: The simulation results in CMP configuration for pipe without leakage	60
Figure 5-27: The simulation results in CMP configuration for pipe leakage with Localized 40% Wet Soil.....	60
Figure 5-28: The simulation results in CMP configuration for pipe leakage with Localized 30% Wet Soil.....	61
Figure 5-30: The simulation results in CMP configuration for pipe leakage with Localized 20% Wet Soil.....	61
Figure 5-31: The simulation results from receiver number 5 for the fourth case simulation with different moisture levels.....	62
Figure 5-32: The simulation domain for the third case.....	63
Figure 5-33: Real and imaginary permittivity for hypothetical material.....	63
Figure 5-34: Real and imaginary Permeability for hypothetical material.....	64
Figure 5-35: The simulation results for the fifth case.....	65
Figure 6-1: Time profile of the received signal with (blue) and without (red) consideration of the material dispersion.....	68
Figure 6-2: Time – Frequency analysis of the recorded signal for non-dispersive (Top) and dispersive (bottom) for the preliminary case.....	68
Figure 6-3: Time profile of the received signals for the first case.....	69
Figure 6-4: Time – Frequency analysis of the recorded signal for 40% case (Top) and 30% case (bottom) for the first case.....	70
Figure 6-5: Time – Frequency analysis of the recorded signal for 20% case (Top) and 10% case (bottom) for the first case.....	70
Figure 6-6: Time profile of the received signals for the fourth case .....	71

Figure 6-7: Time – Frequency analysis of the recorded signal for Pipe only (Top) and Pipe with 40% leakage (bottom) for the fourth case.....72

Figure 6-8: Time – Frequency analysis of the recorded signal for Pipe with 30% leakage (Top) and Pipe with 20% leakage (bottom) for the fourth case.....72

# LIST OF ACRONYMS

<b>Acronym</b>	<b>Meaning</b>
<b>ADE</b>	Auxiliary Differential Equations
<b>CFL</b>	Courant-Friedrich-Levy
<b>CMP</b>	Common Mid Point
<b>EM</b>	Electromagnetic
<b>EMP</b>	Electromagnetic Pulse
<b>FDTD</b>	Finite Difference Time Domain
<b>FDTD-ADE</b>	Finite Difference Time Domain- Auxiliary Differential Equations
<b>GMIPML</b>	Generalized Material-Independent Perfectly Matched Layer
<b>GPR</b>	Ground Penetrating Radar
<b>MIPML</b>	Material-Independent Perfectly Matched Layer
<b>NDT</b>	Non Destructive Testing
<b>PML</b>	Perfect Matching Layer
<b>PVC</b>	Polyvinyl Chloride

<b>RMS</b>	Root Mean Square
<b>SNR</b>	Signal to Noise Ratio
<b>TE</b>	Transverse Electric
<b>TEM</b>	Transverse Electromagnetic
<b>TM</b>	Transverse Magnetic
<b>VMC</b>	Volumetric Water Content

# THESIS ABSTRACT (ENGLISH)

**NAME:** Salem Ali Al-Otaibi  
**TITLE:** Development of Advanced GPR Simulation System  
**MAJOR:** ELECTRICAL ENGINEERING  
**DATE:** JANUARY 2012

Ground Penetrating Radar (GPR) is considered as one of the advanced Non-Destructive Testing (NDT) methods with many applications. In this method, electromagnetic wave is transmitted into materials' surfaces then the reflected signals are interpreted to know the materials properties and their internal content. However, one of the limiting factors of the GPR usefulness is the difficulty associated with received signals interpretation. For GPR system to be effective, there is a need to understand the contribution of different materials properties on the EM wave propagation to extract reliable information from the received signals. The interpretation errors can be minimized once a reliable GPR simulation system with precise materials models is used.

In this thesis, we develop an advanced GPR simulation system using the general polarization FDTD-ADE algorithm. The developed algorithm is capable of simulating two and three dimensional GPR signal propagation through lossy, electric and/or magnetic dispersive or non-dispersive materials. The developed algorithm was validated against previous developed algorithm and analytical solution with excellent agreement. Several cases for different dispersive systems with recent material models were presented. The extracted simulation results were processed using Time-Frequency analysis. General characteristics features have been identified for different wet soil moisture percentages.

# THESIS ABSTRACT (ARABIC)

الاسم: سالم علي العتيبي

العنوان: تطوير نظام محاكاة متقدم للرادار مخترق الأرض

التخصص: الهندسة الكهربائية

التاريخ: يناير 2012

يعتبر الرادار مخترق الأرض أحد الاختبارات اللاإتلافية المتقدمة ذات التطبيقات المتعددة. ويتمثل هذا الاختبار في إرسال موجات كهرومغناطيسية إلى سطوح المواد ومن ثم تحليل وتفسير الإشارات المنعكسة لمعرفة خواص تلك المواد وتكويناتها الداخلية. ولكن أحد العوامل المقننة للاستفادة من الرادار مخترق الأرض هي الصعوبة المرتبطة بتحليل وتفسير تلك الإشارات. ولكي نحصل على نظام رادار فاعل فإننا نحتاج لفهم تأثير خواص المواد على انتشار الموجات الكهرومغناطيسية وهو ما يساعد على استخلاص معلومات ذات موثوقية عالية من الإشارات المستقبلية. يمكن تقليل الأخطاء الناتجة عن تحليل وتفسير تلك الإشارات من خلال استخدام نظام محاكاة يحوي نماذج تمثيلية دقيقة للمواد المستقبلية للموجات.

في هذه الرسالة تم تطوير نظام محاكاة متقدم للرادار مخترق الأرض وذلك باستخدام خوارزمية الاستقطاب العامة لحل المعادلات التفاضلية حسابياً. إن ما يميز الخوارزمية المطورة هي القدرة على محاكاة انتشار موجات الرادار مخترق الأرض في بعدين أو ثلاثة أبعاد وخلال مواد ذات صفات مختلفة كالمواد المثالية والمواد الماصة لطاقة الموجات والمواد ذات التشتيت الكهربي أو التشتيت المغناطيسي أو كليهما.

تم مقارنة الخوارزمية المطورة مع خوارزميات سابقة تحوي نماذج لمواد ذات خواص التشتيت الكهربي وحلول حسابية وكانت النتائج متوافقة بدرجة عالية. كما تم استخدام النظام المطور لمحاكاة انتشار موجات الرادار الأرضي خلال أنظمة تحوي مواد ذات صفات تشتيت مختلفة وممثلة بنماذج مطورة مؤخراً. وكذلك تمت معالجة الإشارات الناتجة من هذه الأنظمة بواسطة التحليل الزمني الترددي لتحديد الصفات المميزة لهذه الإشارات.

درجة الماجستير في العلوم

جامعة الملك فهد للبترول و المعادن

الظهران المملكة العربية السعودية



# INTRODUCTION

## 1.1 Overview

Ground Penetrating Radar (GPR) is a valuable tool for subsurface imaging. It has been used for different applications including land mines detection, soil water content estimation and concrete quality assessment. GPR is also one of the most suitable technological solutions for timely detection of damaged utilities and leakage from pipelines. In basic principle, GPR sends an electromagnetic (EM) wave through an antenna to the ground and receives reflected signals. These received signals can characterize subsurface layers with its buried objects, if any, when interpreted correctly.

The main factor that plays a considerable role on the received GPR signals behavior, is the material electric and magnetic properties through which the GPR signal is propagating. These properties together with the materials configuration, transmitted pulse duration and direction of propagation, influence the GPR transmitted signal through different wave/materials interaction phenomena and contribute to the overall received signals appearance.

The difficulty associated with the GPR received signals interpretation is one of the limiting factors of its usefulness, especially if there is no previous information regarding the tested location. In order to minimize the interpretation errors, reliable GPR simulation system with precise material model is used.

GPR simulation system should be capable of incorporating all possible material properties, particularly material dispersion property. Most materials change their behavior and interactions with EM wave based on the transmitted signal frequency contents. This material property is called material dispersion. Electric and magnetic dispersion are two types of material dispersion that are involved in EM wave propagation problems. This property is a unique property for each material and varies with frequency variation. For example, some materials are known to be strongly dispersive in certain bandwidth. However, they have negligible dispersion in another. This property (either electric or magnetic dispersion) can cause change of signal direction, received time, attenuation and can change the received signal velocity. Electric and magnetic dispersion relations can be modelled using multi-pole Lorentz, Debye or Drude model. The last two models are considered as special cases of Lorentz model.

Most of the devoted work on GPR simulation system development focuses on either non-dispersive materials or Debye electrically dispersive materials. The missed class of materials (electrically dispersive with Lorentz model or magnetically dispersive materials) forms an important class and cannot be neglected when GPR simulation system is needed. This introduces the need to have a general and robust GPR simulation system algorithm that incorporates electric and magnetic dispersive materials with multi-poles Lorentz model.

## 1.2 Literature Review

One of the advanced Non-Destructive Testing (NDT) methods is GPR. GPR is a powerful Non-Destructive sensing tool [1]. It is used in many areas such as geophysics, military technologies, archeology, civil engineering and environmental engineering. GPR has many applications including road pavement analysis [2], void detection [1], location of reinforcement (re-bars) in concrete [3], location of public utilities (pipes, cables, etc)[4], pipe leak detection [5], testing integrity of building materials [3], and minerals exploration [6]. Also, it has been used for measuring the sea ice layer thickness, measuring scouring around bridge supports, generating profile image for lakes bottom side and detecting buried hazardous waste.[7]. Many GPR methods have been used to approximate volumetric water content (VWC) [8]. In GPR studies, the travel time associated with the propagating EM wave between the transmitting antenna and receiving antenna is measured and used to approximate the dielectric permittivity of the tested soil bulk. After that, the approximated dielectric permittivity can be used to estimate the VWC Using a site-specific or general empirical relationship [9] [10].. VWC estimates have been obtained using GPR cross-borehole, ground wave and reflection methods.

In cross-borehole radar method , two dimensional radar wave velocity image is generated between the boreholes. This image is generated using the wave travel time between selected points with marked locations. The wave velocity is used to estimate the dielectric permittivity which is the converted into VWC estimates [11]. Compared to the neutron probes methods, VWC estimates obtained using cross-hole has a Root Mean Square (RMS) error of  $0.03 \text{ m}^3 \text{ m}^{-3}$ [12]. Cross-borehole is a good method for the estimation of VWC for small scale area with lateral extent less than 10 m. Accurate estimation of VWC

for shallow soil can also be obtained using GPR ground wave data [13]. Using this method, VWC was estimated with an RMS error of 0.011–0.017  $\text{m}^3 \text{m}^{-3}$  for 900 and 450 MHz antennas, respectively [13] and 0.024  $\text{m}^3 \text{m}^{-3}$  for 225 MHz antennas [14]. Common-midpoint (CMP) method is also used to estimate the VWC. In this method, central location is identified and radar antenna transmitter and receiver are separated at each side with an equal distance. As the antenna separation increases at each side the travel time of the radar wave increases, which is represented as linear events with slope related to the wave velocity. With CMP method horizontal reflectors appear as hyperbolic reflections on the recorded signals. A non-horizontal reflector will result in a shifted hyperbola on the CMP recorded signals[15]. One of the main limiting factors for the use of CMP as VWC estimation method over large areas, is the needed time to collect the test data. Generally, the associated error of this method is on the order of 10% [16] [17]. Another method for the VWC is the common-offset GPR reflection which can be used only under controlled conditions [18]. In this method artificial reflector is located at a known depth and GPR wave reflections are collected by moving the transmitter and receiver across the ground surface at a fixed distance. After that, the GPR wave travel time to the reflection arrivals is used to determine the average VWC from the ground surface to the reflector. Buried metal plates with known depth was used to estimate VWC to within 0.01  $\text{m}^3 \text{m}^{-3}$  compared to gravimetric water content measurements [19]. Another group estimated VWC using GPR reflected wave from the bottom of a lysimeter with a standard deviation of 0.01  $\text{m}^3 \text{m}^{-3}$ [20]. The significance of GPR as a tool to detect near-surface contaminants is illustrated at a site in the Midwest of USA representing petroleum

product above the water table. Tests show that GPR may provide a means of mapping hydrocarbons in the vadose zone [21].

The purpose of performing GPR simulations is to simultaneously develop novel GPR configurations and detection algorithms for practical applications. Many methods have been proposed and used for the numerical modeling of GPR wave propagation problems. These include ray-based methods [22] frequency-domain methods [23] integral methods [24], and pseudo spectral methods [25]. However, the finite-difference time-domain (FDTD) technique has been used extensively by different researchers for GPR modeling over the past decade as can be seen in [26]-[28]. The FDTD approach has many features over the other methods which includes, capability of accommodating realistic antenna configurations, flexibility in incorporating electric and magnetic dispersion properties, modeling accuracy for complex models [29]. In many published researches [30]-[32], GPR systems operating above conductive and dispersive soil have been simulated. The FDTD approach used to model GPR is a numerical method that provides a solution to Maxwell's equations, expressed in differential form in the time domain. Yee's method [33], is based on the discretization of the partial derivatives in Maxwell's equations using central differencing. The electric( $E$ ) and magnetic( $H$ ) fields are assumed interleaved around a cell whose origin is at the location  $i, j, k$ . Every electric ( $E$ ) field is located at  $1/2$  cell width from the origin in the direction of its orientation. On the other hand, every ( $H$ ) field is at an offset  $1/2$  cell size in each direction except in its orientation direction. An algorithm is developed using the resulting difference equations to solve these equations for the electric and magnetic related quantities and obtain the required solution [34].

Since the development of Yee's original paper, the FDTD method has been used extensively for the solution of electromagnetic field problems such as antenna modeling , electromagnetic pulse (EMP) coupling to dielectric structures, radar cross-section estimations, , electromagnetic field penetration, propagation in plasma and different biological applications. A detailed review of the FDTD method can be found in [35]. FDTD is particularly suitable for solving transient problem such as GPR wave propagation as it is formulated in the time domain[36].Because the FDTD formulation is entirely in the time domain it is particularly suited for solving transient problems such as GPR The simulated region represents only a small area of the actual existed region. Due to this fact, the simulator sees the boundaries that terminate this small region as an interface between two different media that will result in wave reflection. To solve this problem absorbing boundaries should be used. In 1994 J.P. Berenger, proposed the use of Perfect Matching Layer (PML) that dominates all the other absorbing boundaries [37].

### 1.3 Thesis Contribution

The objective of this thesis work is to develop a general and robust GPR simulation algorithm capable of simulating GPR wave propagation through electric and magnetic dispersive or non-dispersive materials with different configurations. Most of the previously developed algorithms were developed for specific dispersion model. However, using the proposed general algorithm, the simulation of different materials with different dispersion models at the same simulation domain can be implemented easily. The incorporation of the magnetic dispersion properties in the developed algorithm, is another major contribution in this thesis as the previously developed algorithms were used for electrically dispersive materials only. To achieve the thesis objective, mathematical derivations were carried out to solve Maxwell's equations numerically to incorporate multi-poles Debye and/or Lorentz dispersive materials. Then the derived equations were translated into a comprehensive two and three-dimensional algorithm.

In the mathematical derivations part, we first consider multi-poles Debye magnetic dispersion relation with magnetic field intensity ( $H$ ). The numerical dispersive relation was derived for this class of materials. The same procedure was followed with multi-poles Lorentz materials. These two relations were incorporated into Maxwell's equations numerically.

Multi-Pole Lorentz electric dispersion relation with electric field intensity ( $E$ ) was also considered. The numerical dispersive relation was derived for this class of materials and incorporated into Maxwell equations.

The developed simulator was used to simulate different cases. Recent wet electric dispersive soil relations with different moisture levels were used in the simulated cases. The dispersion relations were fitted directly to a five-pole Lorentz model. The direct fitting was performed to minimize errors associated with approximated fitting like linear or polynomial fitting.

The simulation results were processed using Time-Frequency analysis. The main goal is to identify some features for different wet soil moisture levels. This signal processing tool has been implemented successfully and distinct features have been identified.

## **1.4 Thesis Organization**

After having an introduction, that includes a review of literature and an insight on the contribution of this thesis work, Chapter 2 gives a general background on GPR. This includes an overview of electromagnetic approach, GPR principles and wave characteristics. Chapter 3 discusses in details basic material dispersion models and recent wet dispersive soil dispersion model. In Chapter 4, FDTD is discussed with detailed numerical representation of Maxwell's equations. The proposed general algorithm for electric and magnetic dispersive materials is also included in this chapter. Chapter 5 presents the simulation results of GPR wave propagation in different dispersive systems with different scenarios using the developed GPR simulators. In Chapter 6, simulation results processed using Time-Frequency analysis are presented. Finally, the thesis concludes with recommendations for future work.



# 2 GROUND PENETRATING RADAR

## 2.1 Introduction

The ability to detect type and location of buried objects has fascinated mankind over centuries. Toward this goal, many methods have been introduced and tested. These methods include seismic, electrical resistivity, induced polarization, gravity surveying, magnetic surveying, nucleonic, radiometric, thermo-graphic and the use of electromagnetic waves [1]. In fact, none of these methods can give full description of the underground layers contents [38]. GPR is one of the most common systems used for this application. It is also used to detect and locate buried objects beneath the ground surface. GPR is a valuable tool for subsurface imaging. It has been used for different applications including land mines detection [39], soil water content estimation [40] and concrete quality assessment [41]. GPR is also one of the most suitable technological solutions for timely detection of damaged utilities and leakage from pipelines [42].

In the following sections, a brief background on the principles of the electromagnetic approach and the principles of the GPR technique are presented.

## **2.2 Principles of Electromagnetic Approach**

In simple terms, the electromagnetic (EM) approach is based on the change in propagation velocity of EM waves upon interacting with material. Material properties are usually defined in terms of permittivity, permeability and conductivity that are, in general, complex quantities. For nonmagnetic soils, permeability is that of vacuum in which the EM waves undergo no magnetic effects. Furthermore, for almost all materials, permittivity, and conductivity vary considerably with the frequency of the propagating wave. The origin of this effect is the induced polarization of atoms and molecules (dipoles) inside the material and the ability of these dipoles to respond to changing fields.

Maxwell's equations are a set of equations that relate the electrical and magnetic fields of the EM wave in different material compositions. These equations were written down in complete form by James Clerk Maxwell. The behavior of the EM waves in any material depends on its electrical and magnetic properties that are represented by three widely used parameters in electromagnetism. These parameters are permittivity, permeability and electrical conductivity. Permittivity is the factor that represents the displacement of bonded charges due to the presence of electric field that results in energy storage in the material in the form of electric field. Permeability is a factor that represents the response of the material to the applied magnetic field that results in storage of energy in magnetic field form. Electrical conductivity characterizes the free charges movement due to external electric field. As these charges move, they face resistance from the material itself that leads to loss of energy.

## 2.3 Principles of GPR

The basic principle of a GPR system is to send an electromagnetic pulse generated by its attached antenna through the ground layers then receive and analyze the reflected signal. The reflected signal (or signals) contains valuable information about the underground layers. A GPR system consists of four main components. The EM wave is generated and transmitted through transmitter antenna in the form of spherical waves that propagate both downward into the ground and upward in the air. The continuity of the wave at the interface gives rise to a lateral wave in the soil. The receiver is an antenna that can detect the reflected EM waves from underground layers and pass them to the processor that applies stored algorithms on these signals to enhance their signal to noise ratio (SNR). Then, these enhanced signals can be shown on display system for interpretation. Figure 2.1 shows a block diagram of a typical GPR system.

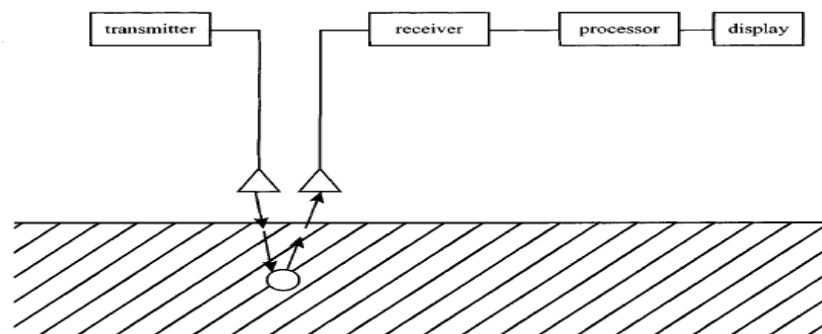


Figure 2.1: Block diagram of typical GPR system[1].

The most important aspects of a GPR system are resolution and penetration depth. Resolution is determined by the frequency content of the transmitted pulse and it increases at shorter central wavelengths. On the other hand, penetration depth is determined by both the soil characteristics and the central wavelength of the transmitted

pulse. In dry sand and gravel, conductivity is low and penetration depth can reach up to few meters at around 1 GHz. For moist soils and clay the penetration depth is significantly less at that frequency.

## 2.4 GPR Wave Characteristics

In order to understand different wave/material interaction phenomena, we should pay a closer look to the wave characteristics and their relationships with intrinsic material properties.

### 2.4.1 Central Frequency

GPR transmitter signal is basically a pulse with finite duration. Since it is a bounded signal, its Fourier transform exists. The wave central frequency (or bandwidth) is approximated by the formula[38]:

$$W \approx \frac{1}{f_c} \approx \frac{1}{B} \quad (2.1)$$

where  $W$  is the pulse width in seconds at half amplitude,  $f_c$  is the central frequency in Hz and  $B$  is the bandwidth in Hz.

The center frequency wavelength is calculated using the formula[38]:

$$\lambda_c = \frac{v}{f_c} \quad (2.2)$$

Where  $v$  is the EM wave velocity in the material.

Central frequency is an important characteristic of GPR wave as it determines the resolution capability of GPR system. GPR resolution consists of two components, namely

the longitudinal (range or depth) resolution length and the lateral (angular or side ways displacement) resolution length see Figure 2.2 for more clarification.

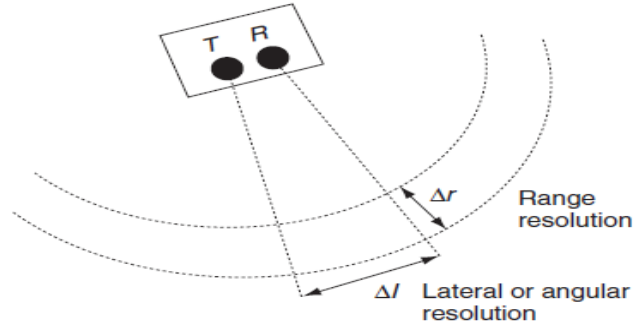


Figure 2.2 Types of GPR resolution [38].

As the GPR signal propagates and faces a reflector, it reflects back and detected by the receiver. This might cause signals overlap. By characterizing a pulse by its width at half amplitude,  $W$ , Rayleigh’s criterion states that two pulses are distinguishable if they are separated by half their “half width”. Hence, if these signals are separated in the time domain by less than this amount, then they might overlap and interpreted as a single pulse. The radial resolution length is expressed as follows[38]:

$$\Delta r \geq \frac{W v}{4} \tag{2.3}$$

where  $v$  is wave speed in meters per seconds.

The lateral resolution length is expressed as follows[38]:

$$\Delta l \geq \sqrt{\frac{d \lambda_c}{2}} \tag{2.4}$$

where  $d$  is the distance from the transmitter to the target in meters.

## 2.4.2 Wave Velocity

Wave velocity is a function of wave frequency and material properties which are characterized by permittivity, permeability and electrical conductivity. These parameters are generally complex quantities. Detailed discussion for material dispersion will be presented in the next chapter. However, we will list their main formulas here[38]:

Complex permittivity

$$\varepsilon^* = \varepsilon' - j\varepsilon'' \quad (2.5)$$

Complex conductivity

$$\sigma^* = \sigma' - j\sigma'' \quad (2.6)$$

Real effective permittivity

$$\varepsilon^e = \varepsilon' - \frac{\sigma''}{\omega} \quad (2.7)$$

Real effective conductivity

$$\sigma^e = \sigma' + \varepsilon''\omega \quad (2.8)$$

Where  $\varepsilon'$  and  $\sigma'$  are the real permittivity and real conductivity, respectively While  $\varepsilon''$  and  $\sigma''$  are the imaginary permittivity and imaginary conductivity, respectively.

The wave velocity is dependent on the signal frequency, effective permittivity and conductivity as follows[38]:

$$v = \frac{c}{\sqrt{\frac{\mu\varepsilon^e}{2} \left[ \sqrt{1 + \left( \frac{\sigma^e}{\omega^2} \right)^2} + 1 \right]}} \quad (2.9)$$

where,

$c$  : is the velocity of EM waves in free space ( $3 \times 10^8$  meters per second)

$\omega$  : angular frequency (rad/second)

### 2.4.3 Wave Attenuation

As the EM wave propagates through lossy materials, it loses some or all of its energy due to wave/material interaction. Wave attenuation depends on wave frequency, material permittivity, permeability and electric conductivity. The below formula is used to calculate wave attenuation[38].

$$\alpha = \omega \sqrt{\mu\varepsilon^e} \sqrt{\left( \frac{1}{2} \left[ \sqrt{1 + \left( \frac{\sigma^e}{\omega^2 \varepsilon^2} \right)^2} - 1 \right] \right)} \quad (2.10)$$

The attenuation unit is Neper/meter.

### **3 MATERIAL DISPERSION MODELS**

In this chapter, a brief description of material dispersion models is presented including the most common types, Lorentz, Debye and Drude. As far as soil models are concerned, the most prominent model for moisture is discussed.

#### **3.1 Material Models**

Most materials change their behavior and interactions with EM wave based on the wave frequency contents. This material property is called material dispersion. Electric and magnetic dispersion are two types of material dispersion that are involved in EM wave propagation problems. This property is a unique property for each material and varies with frequency variation. Several material models have been proposed to describe the frequency response of materials. These models were developed based on the electron motion with respect to the atom nucleus in the presence of external electric field. Once this behavior investigated and understood, a model of the electric susceptibility (or permittivity) of a material can be proposed.. Due to the analogy between electric and magnetic fields, a similar models can be proposed for magnetic susceptibility (or permeability) to incorporate the magnetic dispersion of material. While the magnetic dipoles physically arise from moments associated with current loops, they can be described(mathematically) by magnetic charge and current, analogous to the electric cases. The below sections discuss the main dispersion models.



### 3.1.1 The Lorentz Model.

Lorentz model is the most well-known material dispersion model. It is derived by a description of the electron motion in terms of a driven, damped harmonic oscillator. The charges are assumed to be allowed to move in the electric field direction. The Lorentz model describes the response of a component of the polarization field of a given material to the same component of the external electric field as

$$\frac{d^2}{dt^2} P_i + \Gamma_L \frac{d}{dt} P_i + \omega_0^2 P_i = \epsilon_0 \omega_p^2 E_i \quad (3.1)$$

The first term on the left hand side accounts for the charges acceleration, the second term accounts for the system damping mechanisms with damping coefficient  $\Gamma_L$ , and the third term represent the restoring forces due to the nucleus/electron attraction force where  $\omega_0^2 = S/m$  and  $S$  is the spring constant of the harmonic oscillator and  $m$  is the mass of the charge (see Figure 3.1).

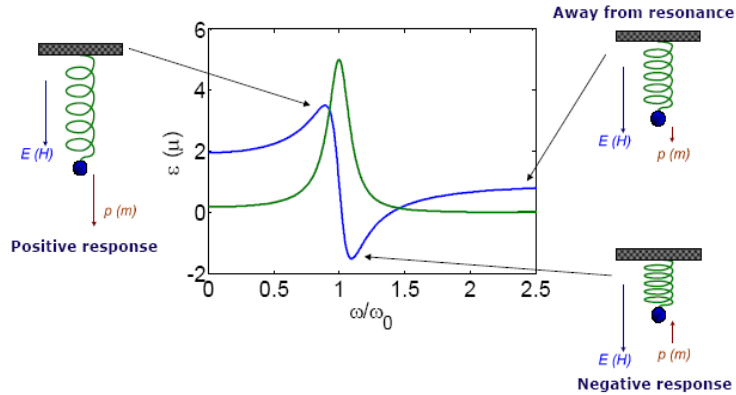


Figure 3.1: Resonance described by the Lorentz model.

The coupling coefficient  $\omega_p$  of the driving term is

$$\omega_p = \sqrt{Nq^2/m\epsilon_0} \quad (3.2)$$

where,  $N$  is the number of charges/molecules per unit volume. The response in the frequency domain, assuming the  $e^{j\omega t}$  time dependence, is given by the expression:

$$P_i(\omega) = \frac{\varepsilon_0 \omega_p^2 E_i(\omega)}{-\omega^2 + j\Gamma_L \omega + \omega_0^2} \quad (3.3)$$

The polarization and electric fields are related to the electric susceptibility as:

$$\chi_{eLorentz}(\omega) = \frac{P_i(\omega)}{\varepsilon_0 E_i(\omega)} = \frac{\omega_p^2}{-\omega^2 + j\Gamma_L \omega + \omega_0^2} \quad (3.4)$$

The permittivity is then obtained as:

$$\varepsilon_{Lorentz}(\omega) = \varepsilon_0 (1 + \chi_{eLorentz}(\omega)) \quad (3.5)$$

The complex relative permittivity is given as:

$$\varepsilon(\omega) = \varepsilon'(\omega) - j\varepsilon''(\omega) \quad (3.6)$$

### 3.1.2 The Drude Model.

The Drude model is a special case of the Lorentz model. Drude model is suitable for a material that doesn't have strong nucleus/electron attraction effect in the presence of external electric field. For such material the restoring force in the Lorentz model can be neglected. The Drude model then describes the response of a component of the polarization field of a given material to the same component of the external electric field as:

$$\frac{d^2}{dt^2} P_i + \Gamma_L \frac{d}{dt} P_i = \varepsilon_0 \omega_{pd}^2 E_i \quad (3.7)$$

The polarization and electric fields are related to the electric susceptibility as:

$$\chi_{eDrude}(\omega) = \frac{P_i(\omega)}{\varepsilon_0 E_i(\omega)} = \frac{\omega_{pd}^2}{-\omega^2 + j\Gamma_L \omega} \quad (3.8)$$

The permittivity is then obtained as:

$$\varepsilon_{Drude}(\omega) = \varepsilon_0 (1 + \chi_{eDrude}(\omega)) \quad (3.9)$$

### 3.1.3 The Lorentz-Drude Model.

Lorentze-Drude model is the most general dispersion model. It incorporates the polarization in a material that have both free and bound electrons. The free electrons have a negligible restoring force , hence its impact can be modeled using Drude model while the polarization due to the bound electrons can be modeled with other term using Lorentz model [36]. The permittivity in the Lorentze-Drude model is given by

$$\mathcal{E} = \mathcal{E}_{free} + \mathcal{E}_{bound} \quad (3.10)$$

For the free electron, permittivity is

$$\mathcal{E}_{free} = 1 + \frac{\omega_p}{j\Gamma\omega + \omega^2} \quad (3.11)$$

and for bound electrons, permittivity is

$$\mathcal{E}_{bound} = \frac{\omega_p}{\omega_0 + j\Gamma\omega + \omega^2} \quad (3.12)$$

Combining both models together, yields

$$D(\omega) = \epsilon_0 \left( 1 + \frac{\omega_p}{j\Gamma\omega - \omega^2} + \frac{\omega_p}{\omega_0 + j\Gamma\omega - \omega^2} \right) E(\omega) \quad (3.13)$$

### 3.1.4 The Debye Model.

In some materials, the acceleration term is small compared to the other terms in Lorentz model. The obtained model when the acceleration term is neglected is Debye model

$$\Gamma_L \frac{d}{dt} P_i + \omega_0^2 P_i = \epsilon_0 \omega_{pdeb}^2 E_i \quad (3.14)$$

The electric susceptibility is then given as

$$\chi_{eDebye}(\omega) = \frac{\omega_{pdeb}^2}{j\Gamma_L\omega + \omega_0^2} \quad (3.15)$$

Debye model assumes that dielectrics are composed of electrical dipoles which change their orientation based on the applied external electric field with some relaxation time (see Figure 3.2). If the applied electric field is oscillating at a low frequency, then the material polarization will be strong. However, if the applied electric field is oscillating at a high frequency then the material polarization will be weak. From another point of view, materials with strong polarization have a short relaxation times and materials with weak polarization have long relaxation times. For example, metals are known to have very short relaxation time . Hence, it has strong polarization. The derivation of the Debye model starts from the response of a dielectric to applied DC electrical field.

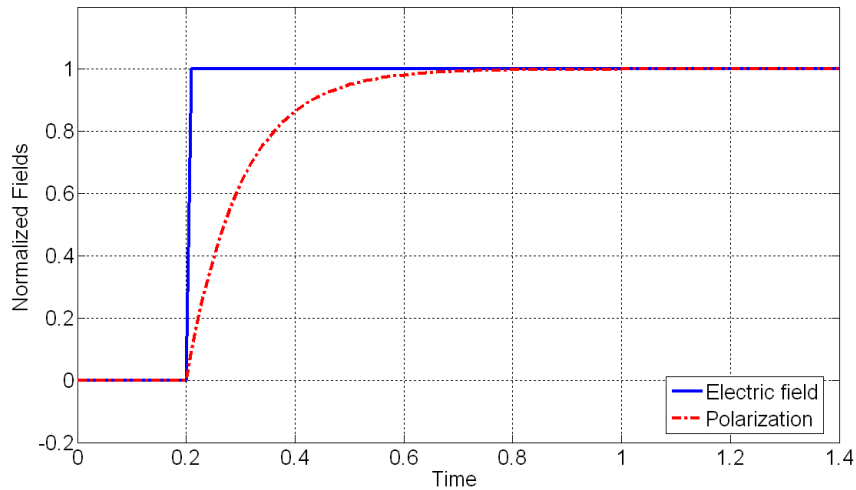


Figure 3.2: Relationship between  $E$  and  $P$  in material Debye modeled dielectric

At steady state electric polarization is given by

$$P(t) = P_{\infty}(1 - e^{-t/\tau}) \quad (3.16)$$

where  $P_{\infty}$  is the polarization in the steady state,  $P(t)$  is the instantaneous polarization and  $\tau$  is the time constant. The derivative of  $P(t)$  starts with

$$\frac{dP(t)}{dt} = \frac{1}{\tau} P_{\infty} e^{-t/\tau} \quad (3.17)$$

Substitution in Equation 3.16 yields

$$P(t) = P_{\infty} - \tau \frac{dP(t)}{dt} \quad (3.18)$$

$P_{\infty}$  can be found using the steady state value of permittivity

$$P(t) = \varepsilon_0 (\varepsilon - 1) E_{\infty} - \tau \frac{dP(t)}{dt} \quad (3.19)$$

Solving for  $E(t)$  gives

$$\varepsilon_0 (\varepsilon - 1) E(t) = P(t) + \tau \frac{dP}{dt} \quad (3.20)$$

Taking the equation to the frequency domain gives

$$\varepsilon_0 (\varepsilon - 1) E(\omega) = P(\omega) + j\omega\tau P(\omega) \quad (3.21)$$

Dividing by  $\varepsilon_0 E(\omega)$  gives

$$\frac{\varepsilon - 1}{(1 + j\omega\tau)} = \frac{P(\omega)}{\varepsilon_0 E(\omega)} = \chi(\omega) \quad (3.22)$$

Thus, the permittivity is given by

$$\varepsilon(\omega) = \chi(\omega) + 1 = \frac{\varepsilon - 1}{(1 + j\omega\tau)} + 1 \quad (3.23)$$

The following condition should be met to ensure optimum fitting of the permittivity function over the frequency range ,

$$\varepsilon(0) = \varepsilon_s \text{ and } \varepsilon(\infty) = \varepsilon_{\infty} \quad (3.24)$$

where,  $\varepsilon_{\infty}$  is the permittivity at infinite frequency and  $\varepsilon_s$  is the static permittivity at DC.

Therefore, the relation has to be modified to be

$$\varepsilon(\omega) = \varepsilon_{\infty} + \frac{\varepsilon_s - \varepsilon_{\infty}}{(1 + j\omega\tau)} \quad (3.25)$$

To take into account the material losses, another term is added to the permittivity. This term is related to the material conductivity.

$$\varepsilon_{realive}(\omega) = \varepsilon_{\infty} + \frac{\varepsilon_s - \varepsilon_{\infty}}{1 + j\omega\tau} - j \frac{\sigma}{\omega\varepsilon_0} \quad (3.26)$$

### 3.2 Soil and Moisture Models

A direct relationship between soil physical properties and the overall dielectric response of the soil constituents (soil particles, water, and air) can be established using dielectric mixing models. It has been shown that four-component mixing model that includes the fraction of bound water associated with high-surface-area clays has resulted in improved prediction of the dielectric response of soils [43]. However, most mixing models developed for soils ignore the imaginary contributions of some or all of the dielectric damping mechanisms associated with bound and bulk soil water [43-47]. Recent soils models by Boyarskii et al. [48] and Mironov et al. [49] include both the real and imaginary components of bound and bulk water. In [48], an empirical fit to measured data is used to approximate bound water relaxation times as a function of water film thickness which facilitates the calculation of the complex permittivity of the bound water component based on the Debye formula.

The soil model that is adopted in this work is a recent application of the four-component dielectric mixing technique that accounts for the contribution of dielectric polarization,  $\varepsilon'(\omega) - j\varepsilon''(\omega)$ , to the complex permittivity of a composite medium with one or more

relaxation processes [50]. The model uses a four-component dielectric mixing model to estimate both  $\epsilon''$  and  $\epsilon'$  with a knowledge of the volumetric fractions of air, soil particles, free water, and water bound to ( or adsorbed by) the surfaces of the soil particles. Using the power-law approximation [43] [45] [51] for  $\epsilon'(\omega) - j\epsilon''(\omega)$  yields the frequency-dependent complex dielectric permittivity given by[50]

$$\epsilon_r(\omega, T) = [\epsilon^*_{air} + \epsilon^*_{soil} + \epsilon^*_{free\ water}(\omega, T) + \epsilon^*_{bound\ water}(\omega, T)]^{1/a} - \frac{j\sigma_o(T)}{\omega\epsilon_o} \quad (3.27)$$

where the effective air dielectric constant is given by

$$\epsilon^*_{air} = \left(1 - \frac{\rho_b}{\rho_s} - \theta\right) (\epsilon_a)^a \quad (3.28)$$

The effective soil dielectric constant is given by

$$\epsilon^*_{soil} = \frac{\rho_b}{\rho_s} (\epsilon_s)^a \quad (3.29)$$

The effective free water dielectric constant is given by

$$\epsilon^*_{free\ water} = (\theta - \theta_{bw}) [\epsilon_{fw}(\omega, T)]^a \quad (3.30)$$

The effective bound water dielectric constant is given by

$$\epsilon^*_{bound\ water} = \theta_{bw} [\epsilon_{bw}(\omega, T)]^a \quad (3.31)$$

In Equation 3.30, we have

$$\epsilon_{fw}(\omega, T) = \epsilon_{\infty} + \frac{\epsilon_{fw \text{ static}}(T) - \epsilon_{\infty}}{1 + j[\omega \tau_{fw}(T)]} \quad (3.32)$$

where

$$\epsilon_{fw \text{ static}}(T) = \frac{3.70886 \times 10^4 - 8.2168 T}{4.21854 \times 10^2 + T} \quad (3.33)$$

and

$$2\pi \tau_{fw}(T) = 1.1109 \times 10^{-10} - 3.284 \times 10^{-12} T + 6.938 \times 10^{-14} T^2 - 5.096 \times 10^{-16} T^3 \quad (3.34)$$

In Equation 3.31, we have[50]

$$\epsilon_{bw}(\omega, T) = \exp\left(\frac{1}{\delta_{bw}} \int_0^{\delta_{bw}} \ln\left\{\epsilon_{\infty} + \frac{\epsilon_{fw \text{ static}} - \epsilon_{\infty}}{[1 + j\omega \tau_{bw}(x, T)]^{\beta}}\right\} dx\right) \quad (3.35)$$

where

$$\delta_{bw} = \frac{10^6 \theta_{bw}}{A_s \rho_b} \quad (3.36)$$

and

$$\tau_{bw}(x, T) = \frac{4\pi r^3 c_o}{KT \exp\left[-\frac{1}{T}\left(\frac{b}{x} + d\right)\right]} \quad (3.37)$$

The temperature-dependent static conductivity is empirically given by[50]

$$\sigma_o(T) = \sigma_{25} \left[ \frac{\theta}{1 - \frac{\rho_b}{\rho_s}} \right]^n [1 + \Delta (T - 298.15)] \quad (3.38)$$

The strategy of using this model is as follows. For any given water content, temperature and soil type, Equation 3.27 is used to generate frequency-dependent data for the complex permittivity. This data is fitted to any standard material model with as many poles as necessary.

As a case study, the parameters in Table 3.1 are used to produce dispersive wet soil real and imaginary permittivity curves for five different percentages as indicated by Figure 3.3 and Figure 3.4.



Table 3.1: Several dispersion types and the corresponding coefficients [50].

<b>Parameters</b>	<b>Description</b>
$a = 0.68$	Exponent of the power-law mixing model
$A_s = 200 \text{ m}^2 \text{ g}^{-1}$	Specific surface area of the soil
$L = 0.2 \text{ m}$	Physical length of the time-domain reflectometry rod
$m = 1$	Exponent to describe the increase in polarization losses with water content
$n = 1.29$	Fitted exponent to describe the increase in bulk electrical conductivity with water content
$p = 20 \text{ m}^3 \text{ m}^{-3}$	Polarization loss factor describing dielectric losses due to bound water
$r = 0.25 \text{ nm}$	Effective radius of water molecule
$T = 298.15 \text{ K}$	Soil temperature
$\beta_{CD} = 1$	Cole–Davidson distribution parameter
$\Delta = 0.0232 \text{ K}^{-1}$	Multiplier to account for the response of the bulk electrical conductivity to temperature
$\delta_L = 0.75 \text{ nm}$	Maximum thickness of the bound water region
$\epsilon_\infty = 3.2$	Dielectric constant of bulk and bound water at infinite frequencies
$\epsilon_a = 1.0$	Relative dielectric permittivity of air
$\epsilon_s = 5.0$	Relative dielectric permittivity of soil solids
$\rho_b = 1350 \text{ kg m}^{-3}$	Bulk density of soil
$\rho_s = 2650 \text{ kg m}^{-3}$	Particle density of soil
$\sigma_{25} = 0.12 \text{ S m}^{-1}$	Bulk electrical conductivity of the soil at saturation and 25° C
$\omega_s = 2.85 \text{ rad GHz}$	Input bandwidth estimated from rise time measurements

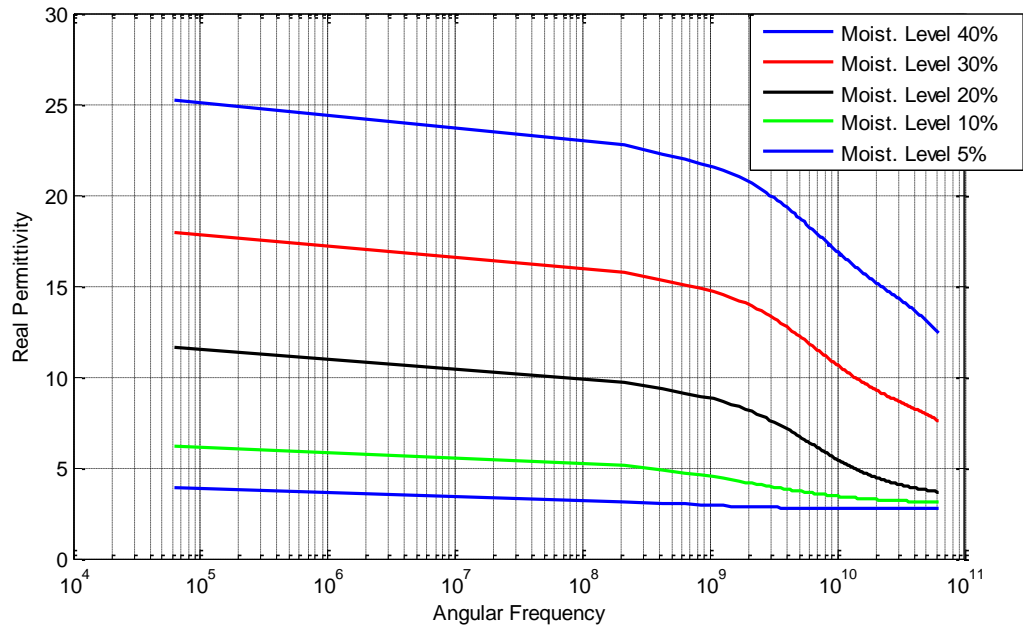


Figure 3.3: Real permittivity curves generated by the empirical model in [50].

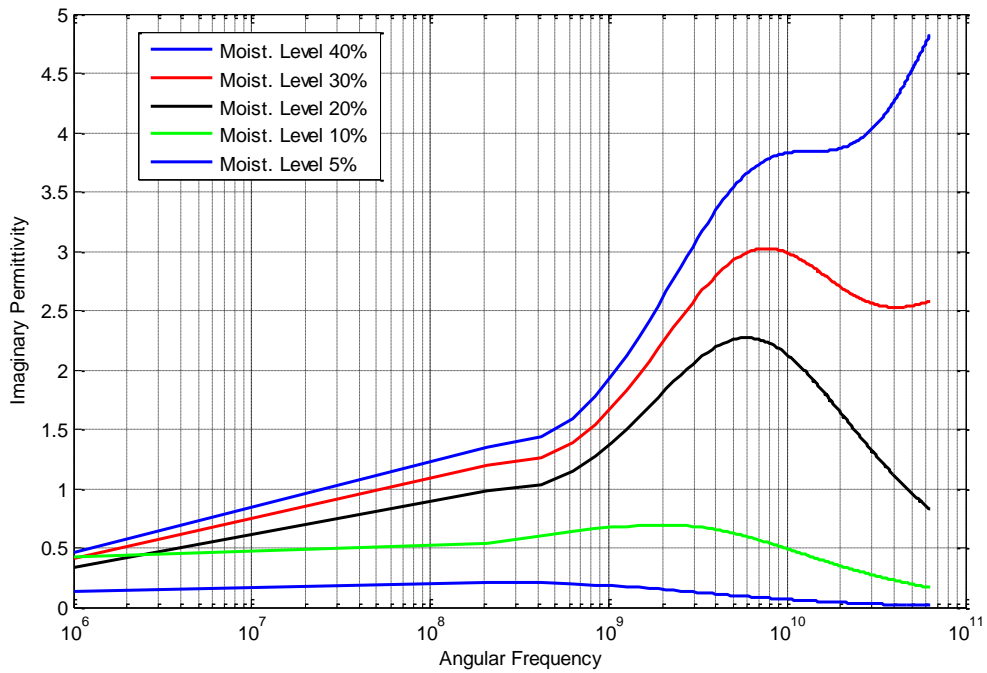


Figure 3.4: Imaginary permittivity curves generated by the empirical model in [50].

## 4 THE FINITE DIFFERENCE TIME DOMAIN METHOD

The Finite-Difference Time-Domain (FDTD) method is one of the most widely used numerical method in the analysis of complex structures in many engineering disciplines and electromagnetic research in particular. In this chapter, a brief description of the simulation method is presented. Also presented is the extension of the method to accommodate the dispersion characteristics of different media.

### 4.1 Introduction to the FDTD Method

The FDTD method is one of the most extensively used numerical methods for the solution of electromagnetic problems. It has many advantages over the other used numerical methods. FDTD has a relatively simple mathematical formulation. Also, it provides an easy way of Maxwell's equations discretization and it does not need any symmetry in the modeled structure. Many researchers introduced different modifications to the FDTD algorithm. The modified versions reduced the computation costs, which grant this method more attention and increase its used in the research activities.

To formulate FDTD in general we need to start with Maxwell's equations. For a non-dispersive (frequency-independent) linear isotropic material, Maxwell's equations can be expressed as

$$\frac{\partial H}{\partial t} = -\frac{1}{\mu} \nabla \times E \quad (4.1)$$

$$\frac{\partial E}{\partial t} = \frac{1}{\varepsilon} \nabla \times H \quad (4.2)$$

Assuming nonmagnetic media (i.e.  $\mu = \mu_o$ ) expansion of the components of the curl operators in Equation 4.1 and Equation 4.2 yield the following six coupled scalar equations in Cartesian coordinates.

$$\frac{\partial E_z}{\partial y} - \frac{\partial E_y}{\partial z} = j\omega\mu_o H_x \quad (4.3a)$$

$$\frac{\partial E_x}{\partial z} - \frac{\partial E_z}{\partial x} = j\omega\mu_o H_y \quad (4.3b)$$

$$\frac{\partial E_y}{\partial x} - \frac{\partial E_x}{\partial y} = j\omega\mu_o H_z \quad (4.3c)$$

$$\frac{\partial H_z}{\partial y} - \frac{\partial H_y}{\partial z} = -j\omega\epsilon_r E_x \quad (4.3d)$$

$$\frac{\partial H_x}{\partial z} - \frac{\partial H_z}{\partial x} = -j\omega\epsilon_r E_y \quad (4.3e)$$

$$\frac{\partial H_y}{\partial x} - \frac{\partial H_x}{\partial y} = -j\omega\epsilon_r E_z \quad (4.3f)$$

These six coupled partial differential Equations (4.3a-f) are used as a base for the FDTD numerical algorithm. The algorithm is modeling the electromagnetic wave interactions with arbitrary three-dimensional medium. The Yee algorithm [33] deals simultaneously with the electric and magnetic fields in time and space, rather than solving the wave equation for either one of them alone.

Yee's proposed a FDTD scheme in which the Maxwell's curl equations were discretized. It first approximates the time and space first-order partial derivatives using central differences, then solves the resulting equations by using a leapfrog scheme [35].

## 4.2 Yee's Orthogonal Mesh

Yee proposed a 3-D mesh having electric and magnetic field components at different locations as shown in Figure 4.1.  $E$  and  $H$  components are located at the centers of the grid lines and surfaces such that each component is surrounded by four field components. This gives a simple representation of three-dimensional space filled with arrays of Faraday's law and Ampere's law contours. Hence, it is possible to identify the  $E$  components which is related to the displacement current flux that links with the  $H$  loops and, similarly, it is possible to identify the  $H$  components which is related to the magnetic flux that links with the  $E$  loops, as shown in Figure 4.1.

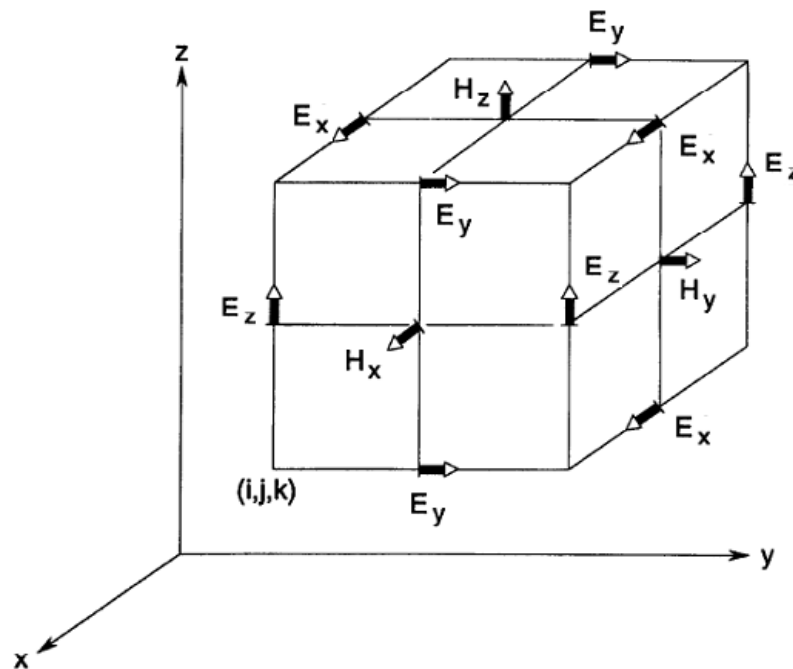


Figure 4.1: Yee's spatial grid.

In case of 2-dimensional space (i.e. of  $x$ - $y$  plane), we will assume that the fields are not varying in the  $z$ -direction, which is represented mathematically as  $\frac{\partial H_y}{\partial z} = 0$ ,  $\frac{\partial H_x}{\partial z} = 0$ ,

$$\frac{\partial E_y}{\partial z} = 0, \frac{\partial E_x}{\partial z} = 0.$$

From Equation 4.3, two independent sets of coupled equations can be obtained.

TM polarized wave:

$$\frac{\partial E_x}{\partial t} = \frac{1}{\varepsilon} \frac{\partial H_z}{\partial y} \quad (4.4a)$$

$$\frac{\partial E_y}{\partial t} = -\frac{1}{\varepsilon} \frac{\partial H_z}{\partial x} \quad (4.4b)$$

$$\frac{\partial H_z}{\partial t} = \frac{1}{\mu} \left( \frac{\partial E_x}{\partial y} - \frac{\partial E_y}{\partial x} \right) \quad (4.4c)$$

and TE polarized wave:

$$\frac{\partial H_x}{\partial t} = -\frac{1}{\mu} \frac{\partial E_z}{\partial y} \quad (4.5a)$$

$$\frac{\partial H_y}{\partial t} = \frac{1}{\mu} \frac{\partial E_z}{\partial x} \quad (4.5b)$$

$$\frac{\partial E_z}{\partial t} = \frac{1}{\varepsilon} \left( \frac{\partial H_y}{\partial x} - \frac{\partial H_x}{\partial y} \right) \quad (4.5c)$$

using Yee's spatial gridding scheme, we can approximate the partial spatial derivatives in Equation 4.4 and Equation 4.5 can by a central difference approximation in the space. For example, Equation 4.4a,4.4b,and 4.4c respectively become

$$\frac{\partial E_x}{\partial t} = \frac{1}{\varepsilon} \frac{H_z(i,j) - H_z(i,j-1)}{\Delta y} \quad (4.6a)$$

$$\frac{\partial E_y}{\partial t} = -\frac{1}{\varepsilon} \frac{H_z(i,j) - H_z(i-1,j)}{\Delta x} \quad (4.6b)$$

$$\frac{\partial H_z}{\partial t} = \frac{1}{\mu} \left( \frac{E_x(i,j+1) - E_x(i,j)}{\Delta y} - \frac{E_y(i+1,j) - E_y(i,j)}{\Delta x} \right) \quad (4.6c)$$

Yee's algorithm also utilizes central differencing in the time domain for the  $E$  and  $H$  components. The  $E$  and  $H$  components are solved using a leapfrog algorithm as shown in Figure 4.2. All of the  $E$  components are computed using the newly computed  $H$  field data and the previously computed values of  $E$ . The computed values are stored for later step usage. At the next step,  $H$  is recomputed based on the newly computed  $E$  field and the previously obtained  $H$ . This process continues until the end of the requested time steps.

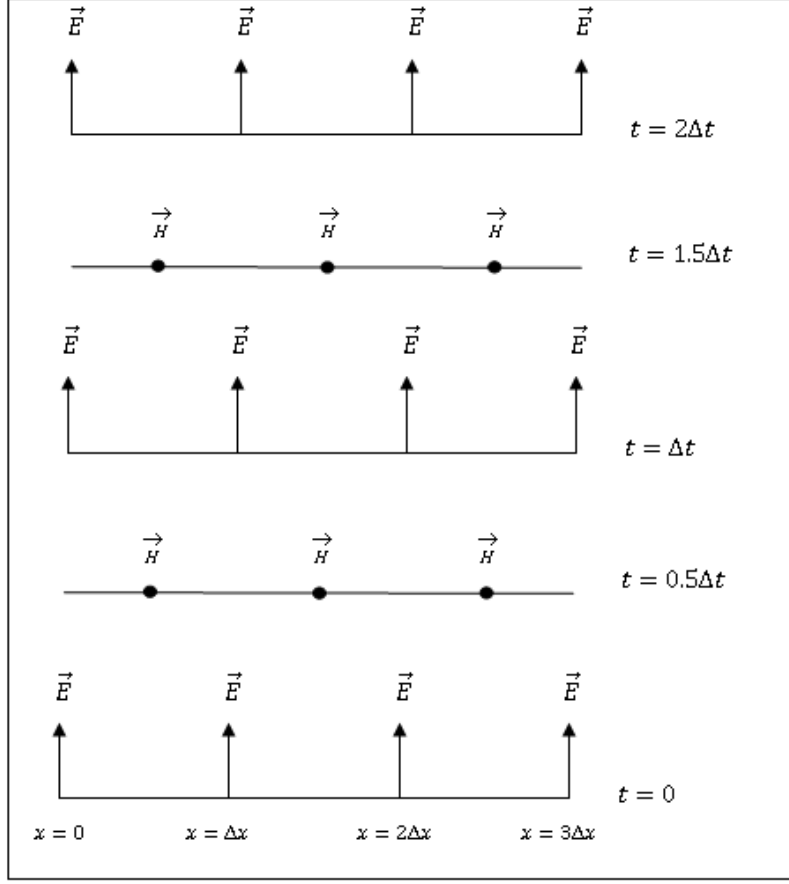


Figure 4.2: Leapfrog temporal scheme of the FDTD method.

Applying central difference approximation, Equations 4.6a-c respectively, become

$$\frac{E_x^{n+1}\left(i+\frac{1}{2},j\right)-E_x^n\left(i+\frac{1}{2},j\right)}{\Delta t} = \frac{1}{\varepsilon} \frac{H_z^{n+\frac{1}{2}}\left(i+\frac{1}{2},j+\frac{1}{2}\right)-H_z^{n+\frac{1}{2}}\left(i+\frac{1}{2},j-\frac{1}{2}\right)}{\Delta y} \quad (4.7a)$$

$$\frac{E_y^{n+1}\left(i,j+\frac{1}{2}\right)-E_y^n\left(i,j+\frac{1}{2}\right)}{\Delta t} = -\frac{1}{\varepsilon} \frac{H_z^{n+\frac{1}{2}}\left(i+\frac{1}{2},j+\frac{1}{2}\right)-H_z^{n+\frac{1}{2}}\left(i-\frac{1}{2},j+\frac{1}{2}\right)}{\Delta y} \quad (4.7b)$$

$$\frac{H_z^{n+\frac{1}{2}}\left(i+\frac{1}{2},j+\frac{1}{2}\right)-H_z^{n-\frac{1}{2}}\left(i+\frac{1}{2},j+\frac{1}{2}\right)}{\Delta t} = \frac{1}{\mu} \left( \frac{E_x^n\left(i+\frac{1}{2},j+1\right)-E_x^n\left(i+\frac{1}{2},j\right)}{\Delta y} - \frac{E_y^n\left(i+1,j+\frac{1}{2}\right)-E_y^n\left(i,j+\frac{1}{2}\right)}{\Delta x} \right) \quad (4.7c)$$

One of the main requirements of the numerical methods is the numerical stability. The time step,  $\Delta t$ , shall have an upper bound to ensure the numerical stability of Yee algorithm. This upper bound is related to the spatial increments  $\Delta x$ ,  $\Delta y$ , and  $\Delta z$  in accordance with the Courant-Friedrich-Levy (CFL) stability condition [35]. In three dimensions, the CFL condition is

$$\Delta t \leq \Delta t_{max} = \frac{1}{c \sqrt{\frac{1}{\Delta x^2} + \frac{1}{\Delta y^2} + \frac{1}{\Delta z^2}}} \quad (4.8)$$

The upper bound on  $\Delta t$  is a sufficient condition to guarantee numerical stability of the subject algorithm.

When simulating propagation of EM waves, the computational domain needs to be terminated. If the simulated region is surrounded by a perfect electric conductor, the termination is achieved by forcing the fields to be equal to zero. However, if the simulated region is not surrounded by a perfect conductor, an error in the computed fields is expected due to the simulation boundary reflection. Berenger [37] proposed a solution to this problem through the introduction of perfectly matched layer (PML). In the PML, the electromagnetic fields are attenuated rapidly when they reach to the simulation boundary until they become equal to zero, which eliminate any expected reflection. To attenuate the EM fields, Berenger introduced two quantities  $\sigma$  and  $\sigma^*$  which are the electrical conductivity and magnetic conductivity, respectively. The resulting equations for TE waves inside the PML are given by

$$\epsilon_0 \frac{\partial E_x}{\partial t} + \sigma E_x = \frac{\partial H_z}{\partial y} \quad (4.9)$$



$$\varepsilon_0 \frac{\partial E_y}{\partial t} + \sigma E_y = -\frac{\partial H_z}{\partial x} \quad (4.10)$$

$$\mu_0 \frac{\partial H_z}{\partial t} + \sigma^* H_z = \left( \frac{\partial E_x}{\partial y} - \frac{\partial E_y}{\partial x} \right) \quad (4.11)$$

To eliminate the reflection between the PML and the simulation region boundary, Berenger assumed that the PML contain a material with the same impedance as the simulation region material. This way the impedance matching principle is met. The condition results in the following equation.

$$\frac{\sigma}{\varepsilon_0} = \frac{\sigma^*}{\mu_0} \quad (4.12)$$

The above illustration solve the reflection problem for normal incidence only. However, due to the nature of the EM wave propagation, the proposed algorithm should deal with all forms of incidence. To solve this problem, the  $H_z$  field shall be split into its sub-fields  $H_{zx}$  and  $H_{zy}$  where one is at normal incidence and the other is tangential to the PML. consequently, the assumed conductivities shall be split which means splitting  $\sigma^*$  to  $\sigma_x^*$  and  $\sigma_y^*$ . Where the first deals with  $H_{zx}$  and the other deals with  $H_{zy}$ . Equation 4.11 will be split into the three equations

$$\mu_0 \frac{\partial H_{zx}}{\partial t} + \sigma_x^* H_{zx} = -\frac{\partial E_y}{\partial x} \quad (4.13)$$

$$\mu_0 \frac{\partial H_{zy}}{\partial t} + \sigma_y^* H_{zy} = \frac{\partial E_x}{\partial y} \quad (4.14)$$

$$H_z = H_{zx} + H_{zy} \quad (4.15)$$

All the mentioned conductivities will not be considered in the computational domain ( $\sigma_x, \sigma_y, \sigma_x^*$  and  $\sigma_y^*$  equal to zero) and will be considered only inside the PML. - This way the PML will work fine for homogenous materials. However, the presence of dispersive and non dispersive material at the PML walls causes a problem.. Zahoet. al. [52] proposed a material independent PML (MIPML) in 1997. The main idea is to apply PML algorithm on a layer that has a field different than electric and magnetic fields which are material dependent fields. He selected to focus on the electric and magnetic flux density fields. Therefore, in the MIPML, the constants involved with both electrical flux density  $D$  and magnetic flux density  $B$  which are material independent fields by their nature are responsible for the PML walls only. Hence, new electrical conductivity  $\sigma$  and magnetic conductivity  $\sigma^*$  are introduced in Maxwell's equations.

$$\frac{\partial D_x}{\partial t} + \sigma D_x = \frac{\partial H_z}{\partial y} \quad (4.16)$$

$$\frac{\partial D_y}{\partial t} + \sigma D_y = -\frac{\partial H_z}{\partial x} \quad (4.17)$$

$$\frac{\partial B_z}{\partial t} + \sigma^* B_z = \left( \frac{\partial E_x}{\partial y} - \frac{\partial E_y}{\partial x} \right) \quad (4.18)$$

Consequently, the impedance matching condition reduces to

$$\sigma = \sigma^* \quad (4.19)$$

This equation indicates that the electric and magnetic conductivity shall be the same. Also, the field splitting should be performed on the  $D$ - $B$  layer. Similar approach could be followed for 3D algorithm.

### 4.3 The General ADE-FDTD Algorithm for Dispersive Materials

The FDTD is a robust numerical method and is used for modeling the EM wave propagation in different materials with complex models. One of the feature of this method, is the capability of incorporating the dispersion properties of the simulated materials.

There are three main techniques to use FDTD with dispersive materials:

1. The recursive convolution (RC) method [53].
2. The auxiliary differential equation (ADE) method [35].
3. The Z-transform method [34].

In my thesis, the ADE dispersive FDTD technique will be discussed in details and will be used to model dispersive materials.

The auxiliary differential equation, first proposed by Taflove [35], was formulated to introduce dispersion relation in FDTD. The ADE method has some features over the other methods which make it widely used for EM problems. ADE method has high flexibility in fitting arbitrary permittivity functions and it gives a more general representation of the dispersion relations. Taflove's proposed to convert the material dispersion relation from the frequency domain into the time domain using Fourier transform. The new  $E$  field will be computed from the previous value of  $E$  and  $D$ . The time domain relation between  $D$  and  $E$  in a dispersive medium, can be extracted using the frequency domain relationship

$$D(\omega) = \epsilon_o \frac{\sigma}{j\omega} E(\omega) \quad (4.20)$$

which can be simplified to

$$j\omega D(\omega) = \varepsilon_o \sigma E(\omega) \quad (4.21)$$

By applying inverse Fourier transform the above equation becomes

$$\frac{dD(t)}{dt} = \varepsilon_o \sigma E(t) \quad (4.22)$$

Discretizing the above relation using forward difference scheme, one gets

$$\frac{D^{n+1} - D^n}{\Delta t} = \varepsilon_o \sigma E^{n+1} \quad (4.22)$$

So the updated E will be

$$E^{n+1} = \frac{D^{n+1} - D^n}{\varepsilon_o \sigma \Delta t} \quad (4.23)$$

The above derivation is efficient for material with single-pole dispersion relation, however for multi-poles materials the equations become difficult to derive. To overcome this problem, Taflove proposed matrix inversion technique. However, using this technique requires a large computational time and memory. The algorithm which was proposed in [54][55] to solve these problem was modified and used to have stable GPR simulation system. In the modified version, only one algorithm is required for any dispersion relation as a result of the ADE method. The dispersive relation has the general form as

$$D(\omega) = \varepsilon(\omega)E(\omega) \quad (4.24)$$

Introducing polarization,  $P$ , one gets

$$D(\omega) = \varepsilon_o \varepsilon_\infty E(\omega) + \sum_i^N P_i(\omega) \quad (4.25)$$

where,  $N$  is the number of poles.

Considering the Lorentzian type as it represents a generalized dispersion form, the polarization field,  $P$ , in the frequency domain can be written as

$$P(\omega) = \frac{a}{b+jc\omega-d\omega^2} E(\omega) \quad (4.26)$$

where  $a$ ,  $b$ ,  $c$  and  $d$  are independent constants representing the material response and unique for each material and  $E$  is the electric field intensity. Equation 4.26 can be rewritten in the following form.

$$[b + c(j\omega) + d(j\omega)^2]P(\omega) = aE(\omega) \quad (4.27)$$

According to the ADE approach, Equation 4.27 the inverse Fourier transform is needed to transform this equation into the time domain

$$bP(t) + c \frac{\partial}{\partial t} P(t) + d \frac{\partial^2}{\partial t^2} P(t) = aE(t) \quad (4.28)$$

Equation 4.28 is solved in the time domain together with Maxwell's curl equations given by

$$\frac{\partial D}{\partial t} = \nabla \times H \quad (4.29)$$

and

$$\frac{\partial B}{\partial t} = -\nabla \times E \quad (4.30)$$

These equations solved using the standard Yee's algorithm. The main step to formulate a consistent and general FDTD algorithm is to approximate the time derivatives in equation 4.28 at each time instant  $n$ . Thus, using central differencing, the following equation can be obtained for  $P$ .

$$bP^n + c \frac{P^{n+1} - P^{n-1}}{2\Delta t} + d \frac{P^{n+1} - 2P^n + P^{n-1}}{\Delta t^2} = aE^n \quad (4.31)$$

Or,

$$P^{n+1} = \frac{4d - 2b\Delta t^2}{2d + c\Delta t} P^n + \frac{-2d + c\Delta t}{2d + c\Delta t} P^{n-1} + \frac{2a\Delta t^2}{2d + c\Delta t} E^n \quad (4.32)$$

$$P^{n+1} = \frac{4d}{2d+c\Delta t} P^n + \frac{-2b\Delta t^2}{2d+c\Delta t} P^n + \frac{-2d+c\Delta t}{2d+c\Delta t} P^{n-1} + \frac{2a\Delta t^2}{2d+c\Delta t} E^n \quad (4.33)$$

Substituting  $P^n$  in the second terms of the right hand side of (4.33) with  $\frac{P^{n+1}+P^{n-1}}{2}$

Equation 4.33 can be written in the form

$$P^n = C_1 P^{n-1} + C_2 P^{n-2} + C_3 E^{n-1} \quad (4.34)$$

Each of these constants  $C_1$ ,  $C_2$  and  $C_3$  is a function of the independent constants  $a$ ,  $b$ ,  $c$  and  $d$  and can be found for each form of dispersion relation. Table 1 gives the expressions for these three constants for different electric dispersion relation including Lorentz, Debye and Drude models. In case of multi-pole dispersion materials, the constants are defined for each pole in the same manner. The updated equation for the electric field intensity is given by

$$E^{n+1} = \frac{D^{n+1} - \sum_i^N P_i^{n+1}}{\epsilon_0 \epsilon_\infty} \quad (4.35)$$

where  $N$  is the number of poles.

Due to the analogy between electric and magnetic fields, the same derivation can be repeated for magnetic dispersive materials. And equations (4.34) (4.35) can be used to calculate Magnetization and the updated magnetic field as per the below equations:

$$M^n = C_1 M^{n-1} + C_2 M^{n-2} + C_3 H^{n-1} \quad (4.36)$$

$$H^{n+1} = \frac{B^{n+1} - \sum_i^N M_i^{n+1}}{u_0 u_\infty} \quad (4.37)$$

The order in which the computations are performed in the general algorithm is shown in the flowchart of Figure 4.3 . First the updated values of the electric flux density fields are

calculated using Equation 4.29. Next, Equation 4.35 is used to calculate the updated electric field where Equation 4.34 is embedded in this calculation. For the magnetic field, first the updated values of the magnetic flux density fields are calculated using Equation 4.30. Next, Equation 4.37 is used to calculate the updated magnetic field where Equation 4.36 is embedded in this calculation.

Table 4.1: Several electric dispersion types and the corresponding coefficients.

Dispersion term in frequency domain	C1	C2	C3
<p><i>Lorentz Pole</i></p> $P = \frac{a}{b + jc\omega - d\omega^2} E$	$\frac{4d}{2d + c\Delta t + b\Delta t^2}$	$\frac{-2d + c\Delta t - b\Delta t^2}{2d + c\Delta t + b\Delta t^2}$	$\frac{2a\Delta t^2}{2d + c\Delta t + b\Delta t^2}$
<p><i>Drude Pole</i></p> $P = \frac{a}{jc\omega - d\omega^2} E$	$\frac{4d}{2d + c\Delta t}$	$\frac{-2d + c\Delta t}{2d + c\Delta t}$	$\frac{2a\Delta t^2}{2d + c\Delta t}$
<p><i>Debye term</i></p> $P = \frac{a}{b + jc\omega} E$	0	$\frac{c\Delta t - b\Delta t^2}{c\Delta t + b\Delta t^2}$	$\frac{2a\Delta t^2}{c\Delta t + b\Delta t^2}$
<p><i>Conductivity term</i></p> $P = \frac{a}{jc\omega} E$	0	1	$\frac{2a\Delta t}{c}$

Table 4.2: Several magnetic dispersion types and the corresponding coefficients.

Dispersion term in frequency domain	C1	C2	C3
<i>Lorentz Pole</i> $M = \frac{a}{b + jc\omega - d\omega^2} H$	$\frac{4d}{2d + c\Delta t + b\Delta t^2}$	$\frac{-2d + c\Delta t - b\Delta t^2}{2d + c\Delta t + b\Delta t^2}$	$\frac{2a\Delta t^2}{2d + c\Delta t + b\Delta t^2}$
<i>Drude Pole</i> $M = \frac{a}{jc\omega - d\omega^2} H$	$\frac{4d}{2d + c\Delta t}$	$\frac{-2d + c\Delta t}{2d + c\Delta t}$	$\frac{2a\Delta t^2}{2d + c\Delta t}$
<i>Debye term</i> $M = \frac{a}{b + jc\omega} H$	0	$\frac{c\Delta t - b\Delta t^2}{c\Delta t + b\Delta t^2}$	$\frac{2a\Delta t^2}{c\Delta t + b\Delta t^2}$

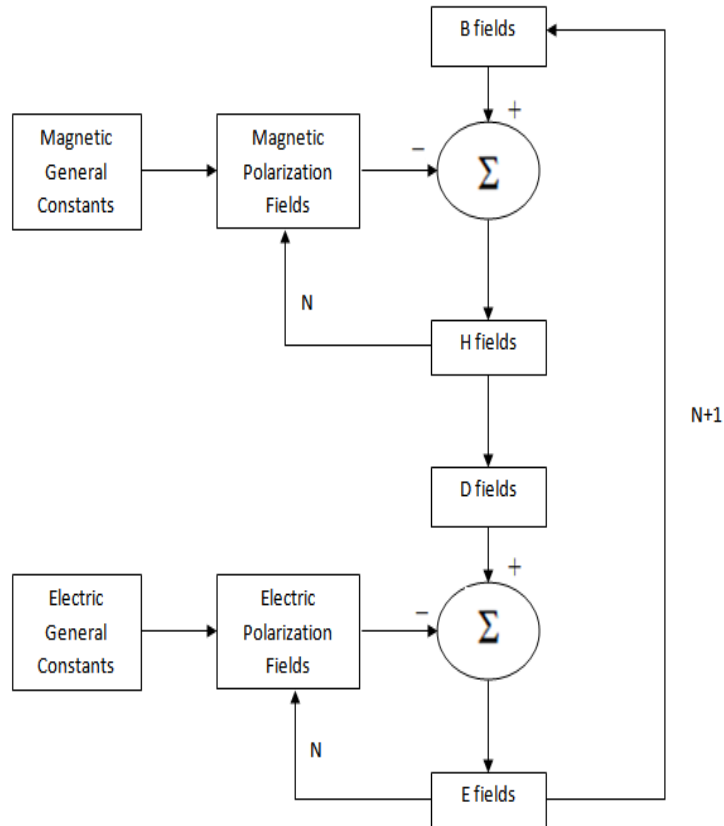


Figure 4.3: A flowchart for the calculations involved in the general algorithm.



## 5 SIMULATION RESULTS

The developed algorithm was implemented using FORTRAN language. Two codes were developed one for 3D system and the other for 2D system. In the next subsections we will present the algorithm validation and selected simulated systems.

### 5.1 Algorithm Validation

The developed algorithm was validated against analytical solution and a previous algorithm developed for GPR system with Debye dispersive material. The case reported by Teixeira et. al. [56] is simulated. The soil dispersion model parameters are obtained by fitting 2-pole Debye and 1-pole conductivity models to the experimental data reported by Hipp [57] for the Puerto Rico type of claim loams. These parameters are given in Table 5.1. The structure is excited with a pulse that is the first derivative of a slightly different version of the Blackmann–Harris pulse [58] so that the pulse vanishes completely after about 8 ns (see Figures 5.1 and 5.2).

The soil region occupies 60% of the vertical height of the simulation domain as shown in Figure 5.3. The field is monitored inside the soil so that it is more sensitive to its dispersive properties. The results shown in Figure 5.4& 5.5 indicate an agreement between the simulation and the published data[56].

Table 5.1: Soil model reported in [57].

Moisture level %	$\epsilon_{\infty}$	$\sigma$ (mS/m)	$A_1$	$A_2$	$\tau_1$ (ns)	$\tau_2$ (ns)
5	4.15	1.11	1.80	0.6	3.79	0.151

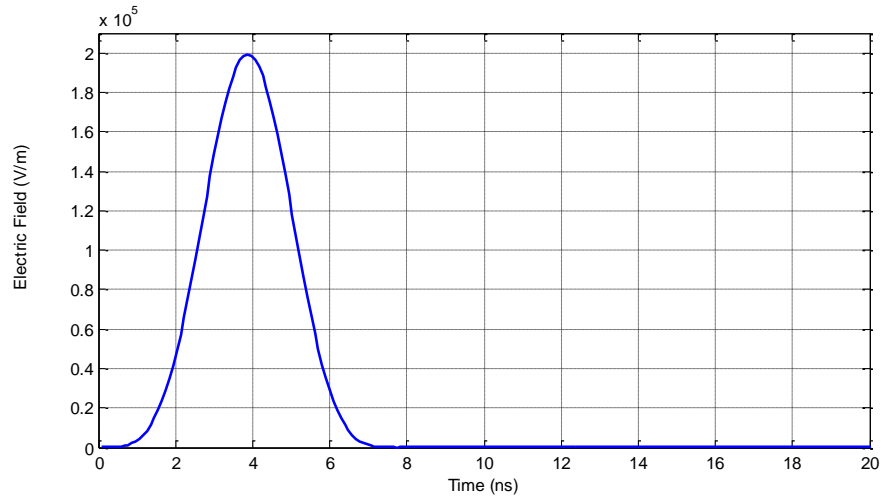


Figure 5.1: Time profile of the signal launched by the transmitter.

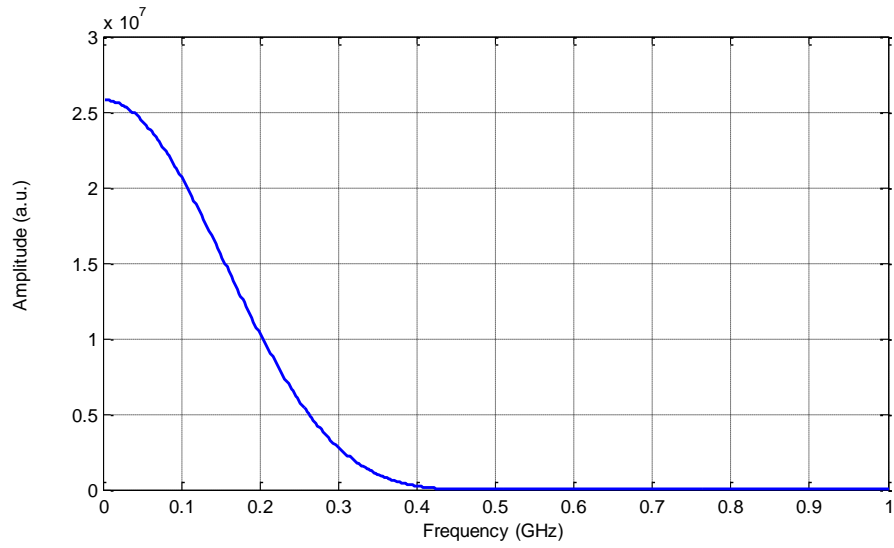


Figure 5.2: The frequency spectrum of the transmitted signal.

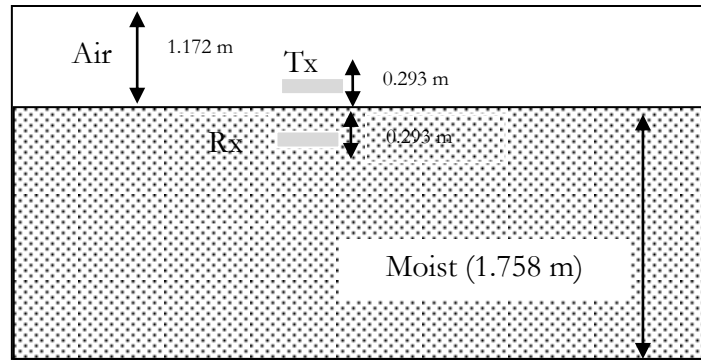


Figure 5.3: The simulation domain for the validated case.

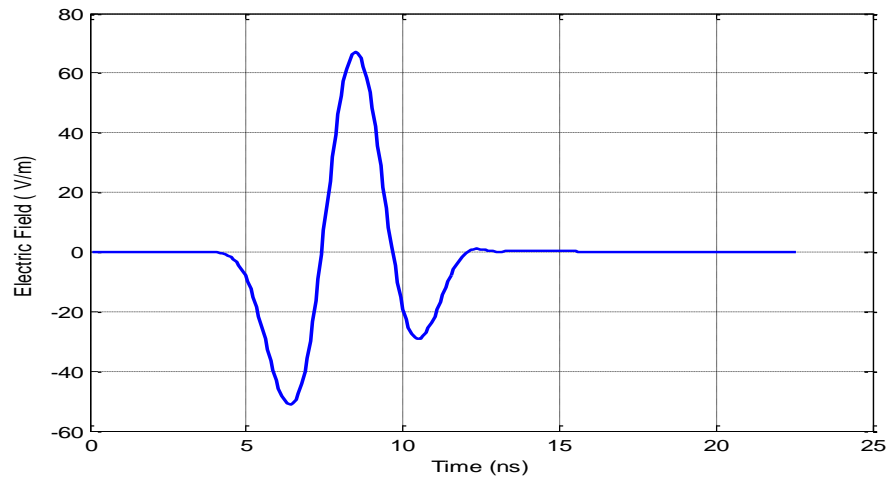


Figure 5.4: Time profile of the recorded electric field (3D simulator).

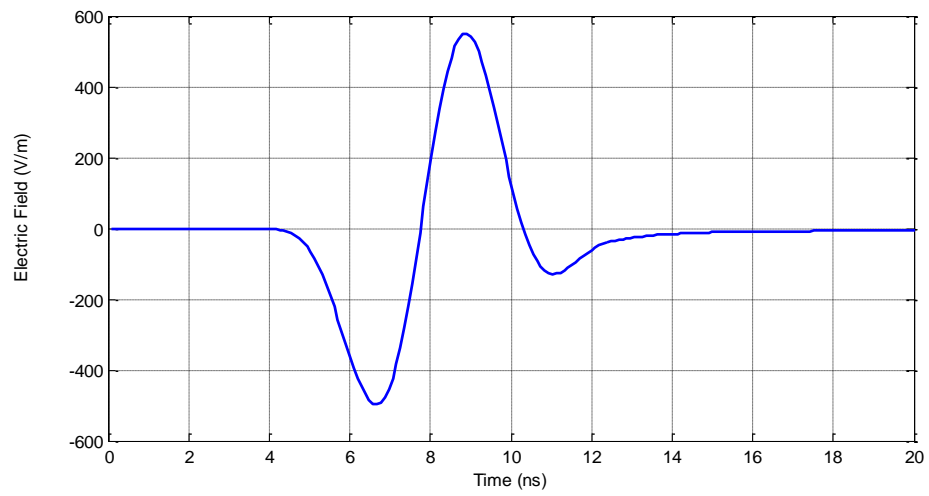


Figure 5.5: Time profile of the recorded electric field (2D simulator).

## 5.2 Simulated Cases

The 2D simulator was used to simulate different electrically dispersive system with materials modeled using multi-pole Lorentz model. For all simulated system, the dimension is five by five meters with PML absorbing boundaries. Also, the field source is considered to be a point source exciting electric field in the x-direction located at 30 cm above the air/ground interface. Several scenarios of the location and extent of the underground moisture region including two layers, three layers and limited moisture regions are investigated. The main dispersive material in the simulated systems is wet soil. As discussed in Section 3.2, recent experimental work reported wet soil electric dispersion relation with five different moisture percentages. The first step to use the reported results is to fit these results to one of the discussed dispersion models.

### 5.2.1 Curve Fitting

Each of the reported relations which were presented in Figure 3.3 and Figure 3.4 were fitted directly to five-pole Lorentz model see Equation 5.1. The extracted parameters were used in the next simulated cases. Table 5.2 shows the optimum parameters that were chosen to fit these relations. Figures 5.6-5.10 show the fitted and report relations. The figures show that the selected parameters fitted the reported relation with excellent

$$\text{agreement. } \varepsilon_r(\omega) = \varepsilon_{inf} + \sum_{i=1}^5 \frac{G_i (\varepsilon_s - \varepsilon_{\infty}) \omega_o^2}{\omega_o^2 + 2j \delta \omega - d \omega^2} \quad (5.1)$$

Where,  $\varepsilon_{inf}$  is the infinite frequency permittivity ,  $G_i$  is the model weight factor ,  $\varepsilon_s$  is the pole static permittivity ,  $\varepsilon_{\infty}$  is the pole infinite frequency permittivity ,  $\omega_o$  is the resonant frequency and  $2 \delta$  is the damping coefficient.

Table 5.2: Multi-pole Lorentz selected parameters wet dispersive soil relations.

Moisture Level	1st Pole	2nd Pole	3rd Pole	4th Pole	5th Pole
5 % $\varepsilon_{inf} = 2.3$	$G_1 = 0.2$	$G_2 = 0.2$	$G_3 = 0.2$	$G_4 = 0.2$	$G_5 = 0.2$
	$\varepsilon_s = 2.8$	$\varepsilon_s = 2.8$	$\varepsilon_s = 2.8$	$\varepsilon_s = 2.8$	$\varepsilon_s = 2.8$
	$\varepsilon_{\infty} = 1$	$\varepsilon_{\infty} = 1$	$\varepsilon_{\infty} = 1$	$\varepsilon_{\infty} = 1$	$\varepsilon_{\infty} = 1$
	$\omega_o = 13$	$\omega_o = 20$	$\omega_o = 13$	$\omega_o = 10.5$	$\omega_o = 12$
	$\delta = 1 \times 10^{-6}$	$\delta = 15 \times 10^{-4}$	$\delta = 5 \times 10^{-6}$	$\delta = 55 \times 10^{-9}$	$\delta = 1 \times 10^{-9}$
	$d = 1 \times 10^{-25}$	$d = 1 \times 10^{-25}$	$d = 1 \times 10^{-25}$	$d = 1 \times 10^{-25}$	$d = 1 \times 10^{-25}$
10 % $\varepsilon_{inf} = 3$	$G_1 = 0.2$	$G_2 = 0.2$	$G_3 = 0.2$	$G_4 = 0.2$	$G_5 = 0.2$
	$\varepsilon_s = 6$	$\varepsilon_s = 6$	$\varepsilon_s = 7$	$\varepsilon_s = 7$	$\varepsilon_s = 5$
	$\varepsilon_{\infty} = 2.5$	$\varepsilon_{\infty} = 1.3$	$\varepsilon_{\infty} = 2$	$\varepsilon_{\infty} = 2.4$	$\varepsilon_{\infty} = 2$
	$\omega_o = 13$	$\omega_o = 20$	$\omega_o = 13$	$\omega_o = 10.5$	$\omega_o = 12$
	$\delta = 1 \times 10^{-6}$	$\delta = 15 \times 10^{-4}$	$\delta = 5 \times 10^{-6}$	$\delta = 55 \times 10^{-9}$	$\delta = 3 \times 10^{-8}$
	$d = 1 \times 10^{-25}$	$d = 1 \times 10^{-25}$	$d = 1 \times 10^{-25}$	$d = 1 \times 10^{-25}$	$d = 1 \times 10^{-25}$
20 % $\varepsilon_{inf} = 5$	$G_1 = 0.1$	$G_2 = 0.2$	$G_3 = 0.2$	$G_4 = 0.2$	$G_5 = 0.3$
	$\varepsilon_s = 10$	$\varepsilon_s = 10$	$\varepsilon_s = 8$	$\varepsilon_s = 8$	$\varepsilon_s = 10$
	$\varepsilon_{\infty} = 2$	$\varepsilon_{\infty} = 2$	$\varepsilon_{\infty} = 3$	$\varepsilon_{\infty} = 3$	$\varepsilon_{\infty} = 2$
	$\omega_o = 13$	$\omega_o = 13$	$\omega_o = 13$	$\omega_o = 13$	$\omega_o = 12$
	$\delta = 17 \times 10^{-7}$	$\delta = 15 \times 10^{-7}$	$\delta = 1 \times 10^{-7}$	$\delta = 2 \times 10^{-8}$	$\delta = 2 \times 10^{-8}$
	$d = 1 \times 10^{-25}$	$d = 1 \times 10^{-25}$	$d = 1 \times 10^{-25}$	$d = 1 \times 10^{-25}$	$d = 1 \times 10^{-25}$
30 % $\varepsilon_{inf} = 9$	$G_1 = 0.1$	$G_2 = 0.2$	$G_3 = 0.2$	$G_4 = 0.2$	$G_5 = 0.3$
	$\varepsilon_s = 9$	$\varepsilon_s = 9$	$\varepsilon_s = 12$	$\varepsilon_s = 14$	$\varepsilon_s = 13$
	$\varepsilon_{\infty} = 2$	$\varepsilon_{\infty} = 2$	$\varepsilon_{\infty} = 1$	$\varepsilon_{\infty} = 1$	$\varepsilon_{\infty} = 1$
	$\omega_o = 13$	$\omega_o = 13$	$\omega_o = 13$	$\omega_o = 13$	$\omega_o = 13$
	$\delta = 17 \times 10^{-7}$	$\delta = 21 \times 10^{-7}$	$\delta = 22 \times 10^{-7}$	$\delta = 5 \times 10^{-8}$	$\delta = 1 \times 10^{-8}$
	$d = 1 \times 10^{-25}$	$d = 1 \times 10^{-25}$	$d = 1 \times 10^{-25}$	$d = 1 \times 10^{-25}$	$d = 1 \times 10^{-25}$
40 % $\varepsilon_{inf} = 12.5$	$G_1 = 0.15$	$G_2 = 0.15$	$G_3 = 0.1$	$G_4 = 0.2$	$G_5 = 0.4$
	$\varepsilon_s = 25$	$\varepsilon_s = 25$	$\varepsilon_s = 21$	$\varepsilon_s = 25$	$\varepsilon_s = 25$
	$\varepsilon_{\infty} = 12$	$\varepsilon_{\infty} = 13$	$\varepsilon_{\infty} = 17$	$\varepsilon_{\infty} = 12$	$\varepsilon_{\infty} = 12$
	$\omega_o = 15$	$\omega_o = 15$	$\omega_o = 15$	$\omega_o = 15$	$\omega_o = 15$
	$\delta = 9 \times 10^{-7}$	$\delta = 1 \times 10^{-7}$	$\delta = 1 \times 10^{-8}$	$\delta = 5 \times 10^{-9}$	$\delta = 1.5 \times 10^{-8}$
	$d = 1 \times 10^{-25}$	$d = 1 \times 10^{-25}$	$d = 1 \times 10^{-25}$	$d = 1 \times 10^{-25}$	$d = 1 \times 10^{-25}$

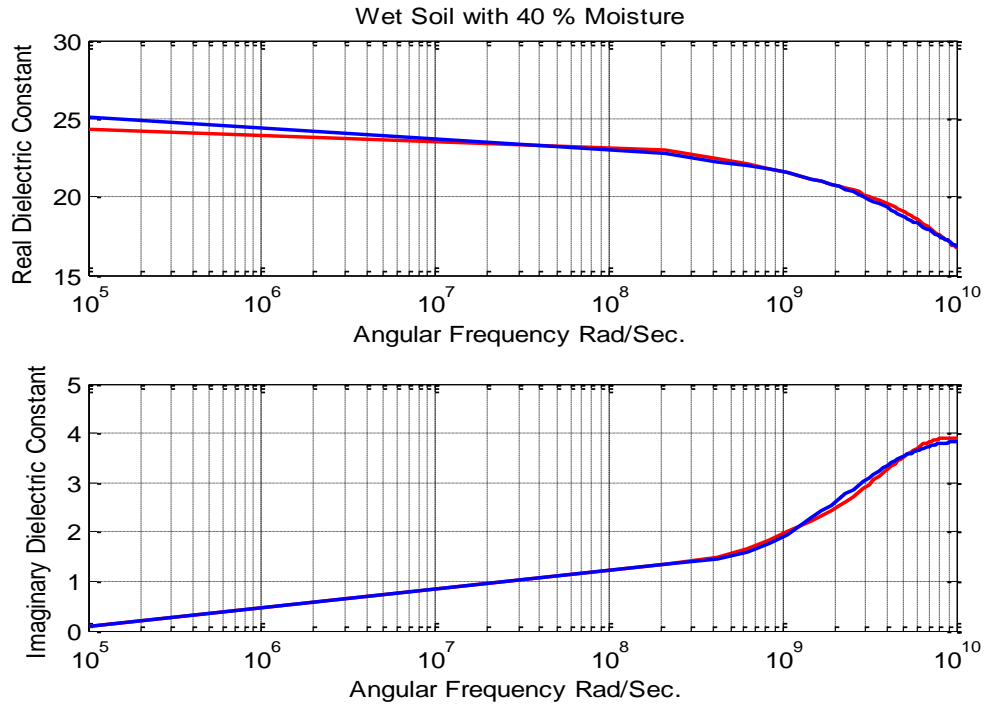


Figure 5.6: Real and imaginary permittivity for wet soil with 40 % moisture generated by the empirical dielectric function (blue) and the corresponding 5-pole Lorentz fit (red).

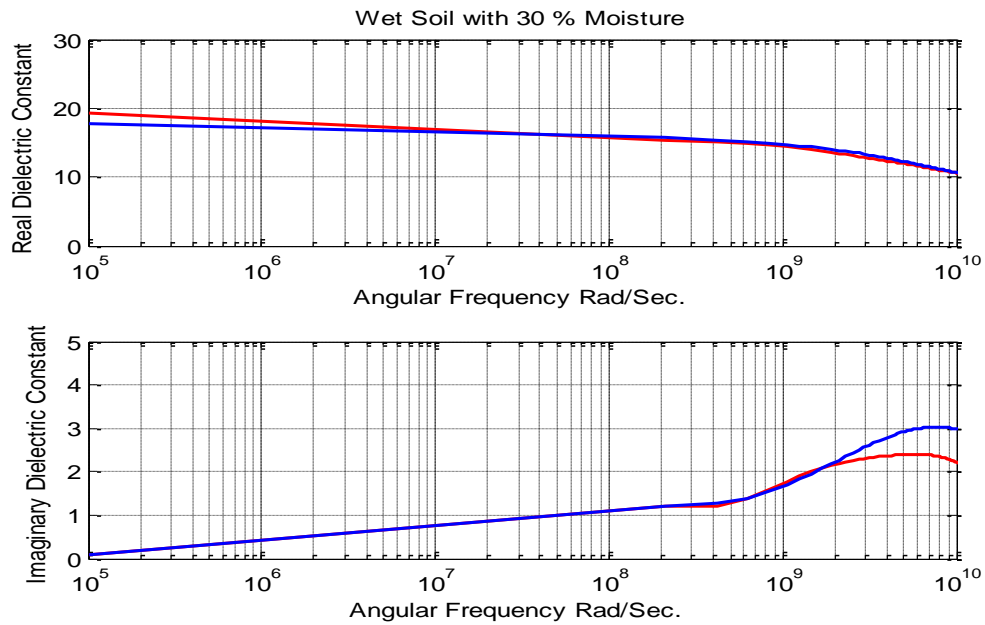


Figure 5.7: Real and imaginary permittivity for wet soil with 30 % moisture generated by the empirical dielectric function (blue) and the corresponding 5-pole Lorentz fit (red).

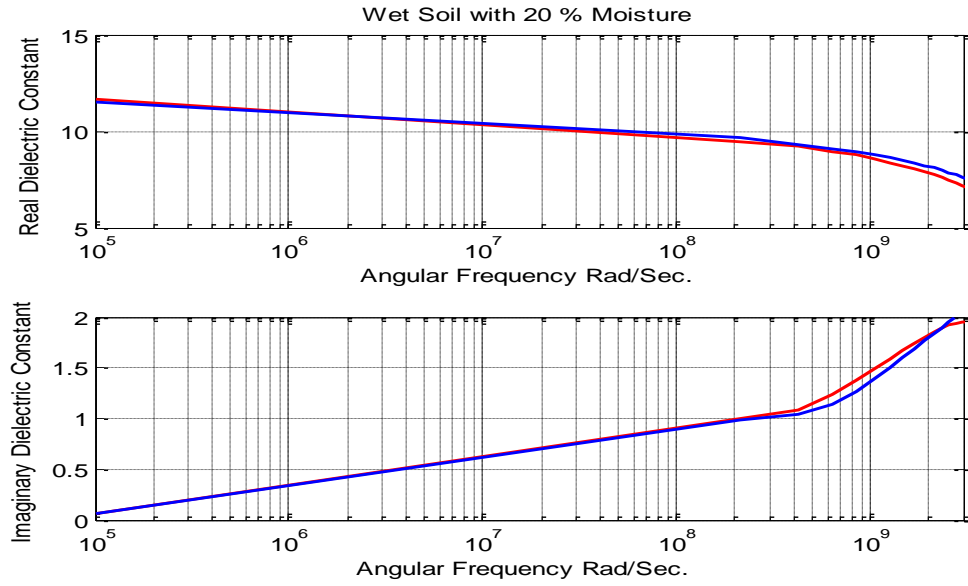


Figure 5.8: Real and imaginary permittivity for wet soil with 20 % moisture generated by the empirical dielectric function (blue) and the corresponding 5-pole Lorentz fit (red).

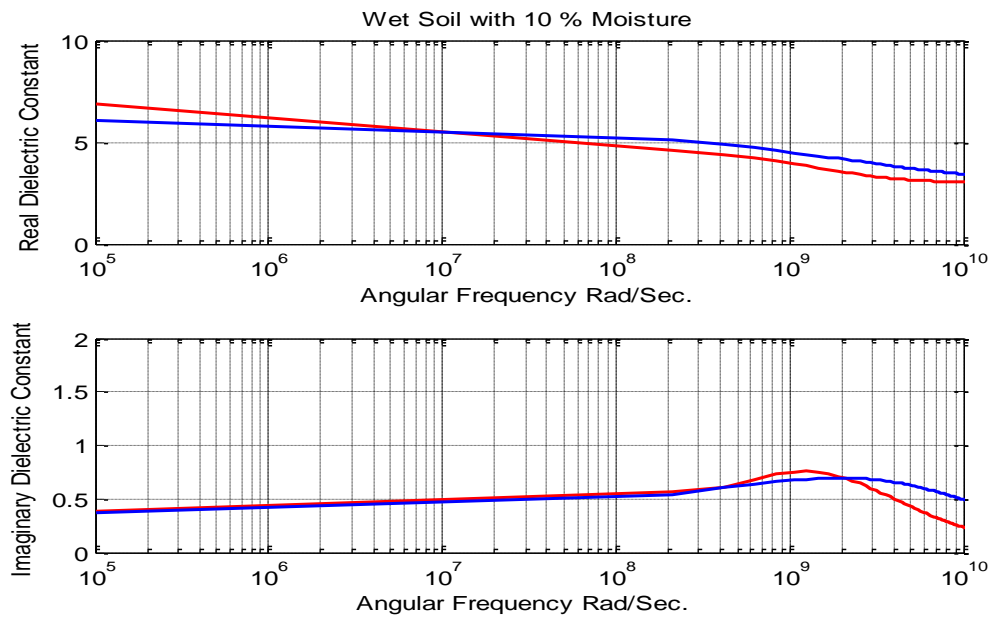


Figure 5.9: Real and imaginary permittivity for wet soil with 10 % moisture generated by the empirical dielectric function (blue) and the corresponding 5-pole Lorentz fit (red).

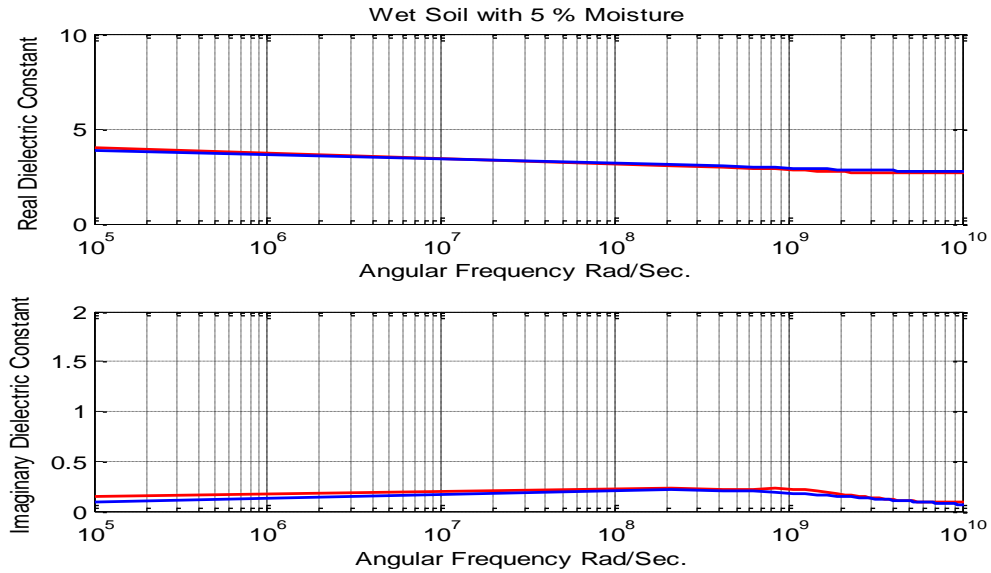


Figure 5.10: Real and imaginary permittivity for wet soil with 5 % moisture generated by the empirical dielectric function (blue) and the corresponding 5-pole Lorentz fit (red).

As it is clear from these curves, the used dispersive wet soil has clear dispersion behavior around one GHz. The used GPR signal should have a central frequency close to one GHz in order to be able to interact with the dispersion properties of these types of soil. Figure 5.11 shows the used pulse. The Fourier transform of this pulse is shown in Figure 5.12.

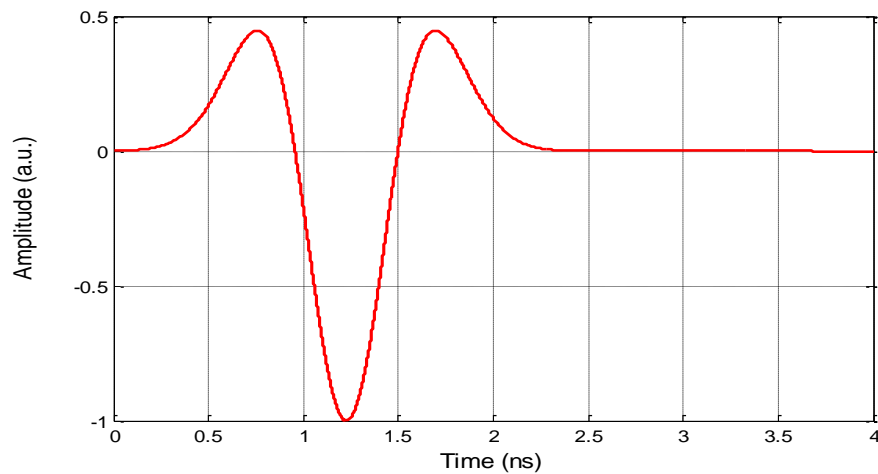


Figure 5.11: Time profile of the signal launched by the transmitter.



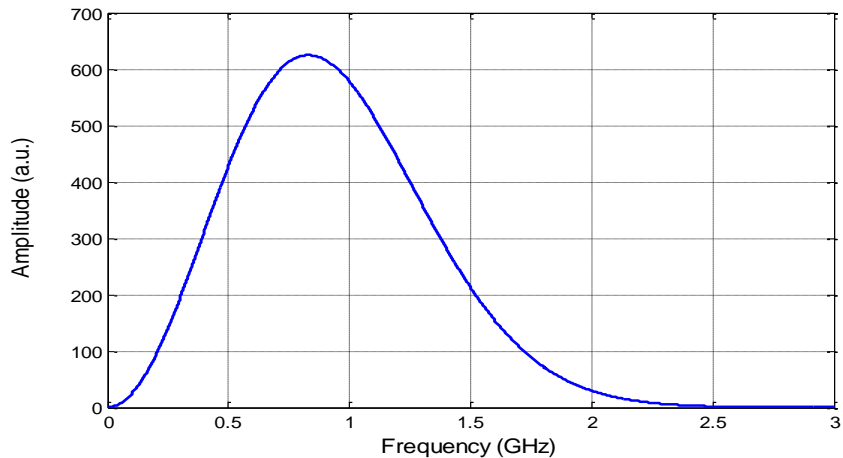


Figure 5.12: The frequency spectrum of the transmitted signal.

### 5.2.2 Preliminary Case: Dispersion Effect

In this introductory case, we simulate GPR wave propagation in dispersive and non-dispersive layer with system similar to the Figure 5.3 system. The GPR signal was recorded in both cases from a point located 20 cm below the air/ground interface . The main objective of the case is to study the influence of electric dispersion on the EM wave propagation. Figure 5.13 shows the recorded signal in both cases. The recorded signal for dispersive signal has a delay compared to the non-dispersive one. This delay is a characteristic feature of dispersive materials compared to non-dispersive ones. Another observation is the amplitude of the recorded signals. It is noticed that for dispersive case the signal inside the layer has less amplitude (energy) compared to the non-dispersive one. This indicates that the signal losses will be higher for dispersive system compared to non-dispersive.

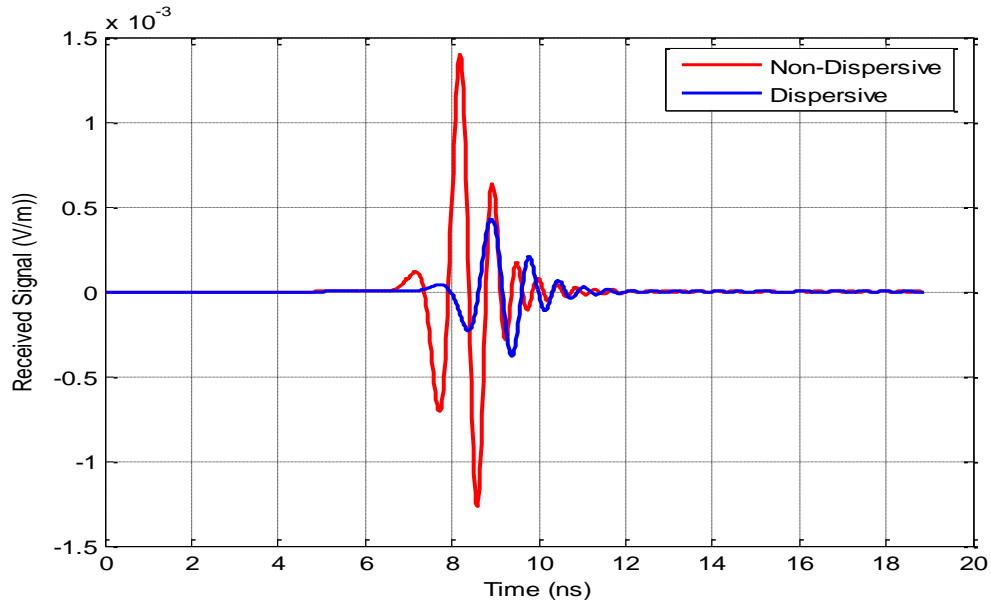


Figure 5.13: Time profile of the received signal with (blue) and without (red) consideration of the material dispersion.

### 5.2.3 First Case : Simulation of a Two-Layer System

This is the simplest case that was implemented. GPR wave propagation was simulated in a system composed of two layers. The first layer is air while the second layer is dispersive wet soil (see Figure 5.14). The simulation was carried out four times with each time different moisture level was used. The main objective of these simulations is to test the GPR system sensitivity to distinguish between different moisture levels in the dispersive wet soil and to look for time domain characteristic features.

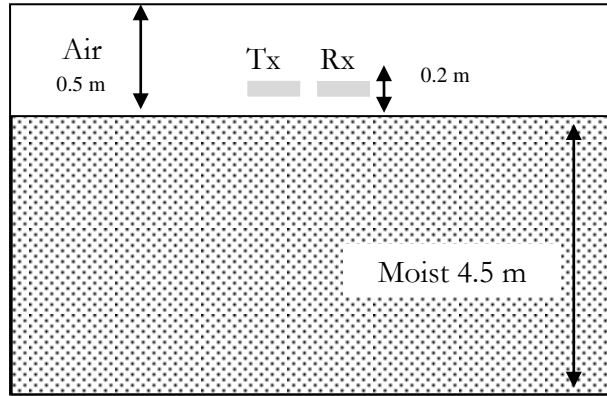


Figure 5.14: The simulation domain for the first case.

Figure 5.15 shows the time profile of the received signal for different moisture levels. The receiver was placed in the middle of the air layer. As expected, higher moisture levels present higher permittivity and hence higher reflections. The overall effects produce distinct features in the time-domain signal such as delay and period of oscillation. The higher moisture level signal has relatively sharper wave transition than the one with lower moisture levels, this suggests that the higher level moisture signals have higher frequency content in time domain transition signal than the lower moisture levels. As the second layer does not contain any reflector (buried objects, localized layer with different EM properties, etc.) no conclusion can be stated for energy absorption in these layers.

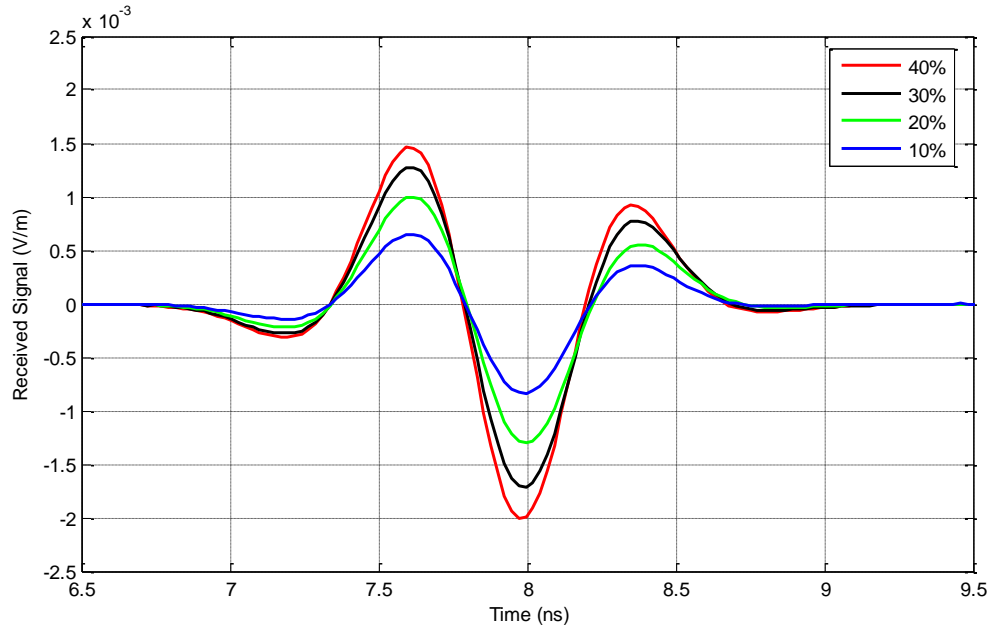


Figure 5.15: Time profile of the received signal for different moisture levels excluding the direct path peak.

#### 5.2.4 Second Case: Simulation of Four Layers

In the second simulation, a system consisting of four layers is used. The first layer is air where the transmitter and receivers are located. Receivers were located in an equi-spaced distance from both sides of the transmitter to achieve CMP configuration. The second and the fourth layer is identical non-dispersive dry sand layer, while the third layer is dispersive wet soil with 40% moisture (Figure 5.16). The simulations were carried out three times where each time the thickness of the third and fourth layer was changed. Figures 5.17-5.18,5.19 present the simulation results in CMP configurations while Figure 5.20 shows a central receiver signal located 2 cm from the transmitter.

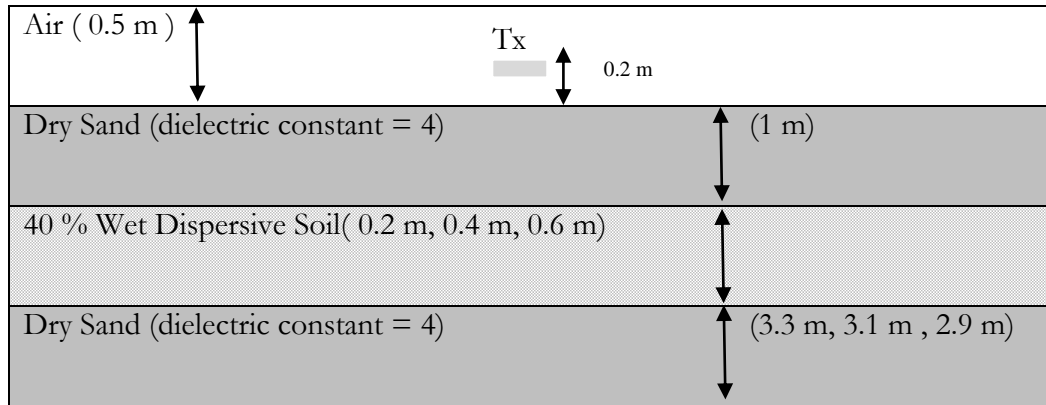


Figure 5.16: The simulation domain for the second case.

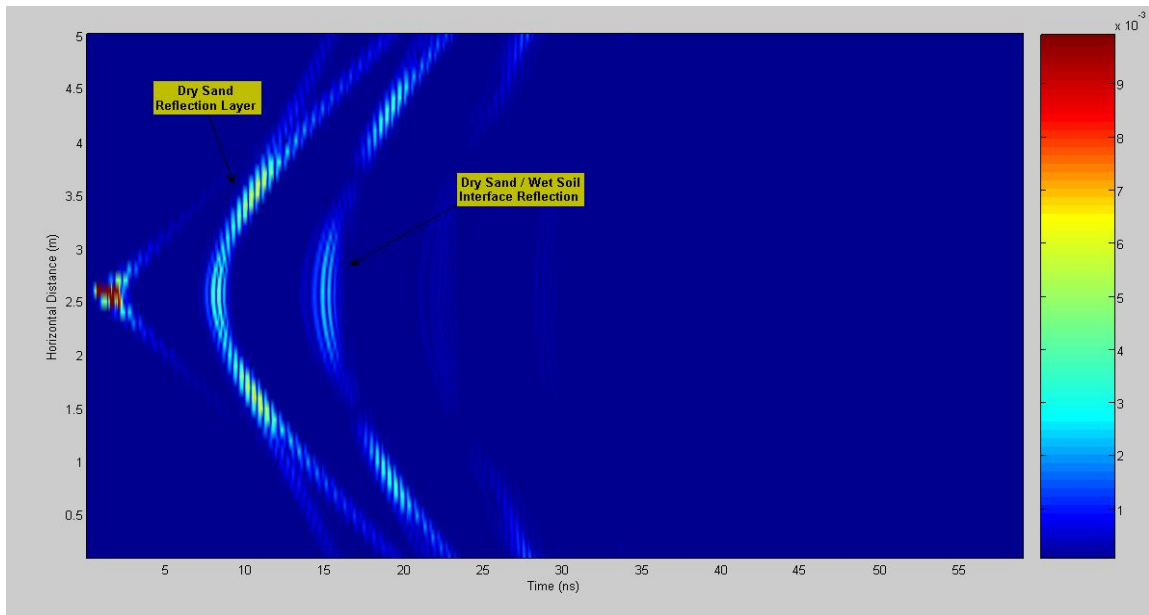


Figure 5.17: The simulation results in CMP configuration with 20 cm wet soil.

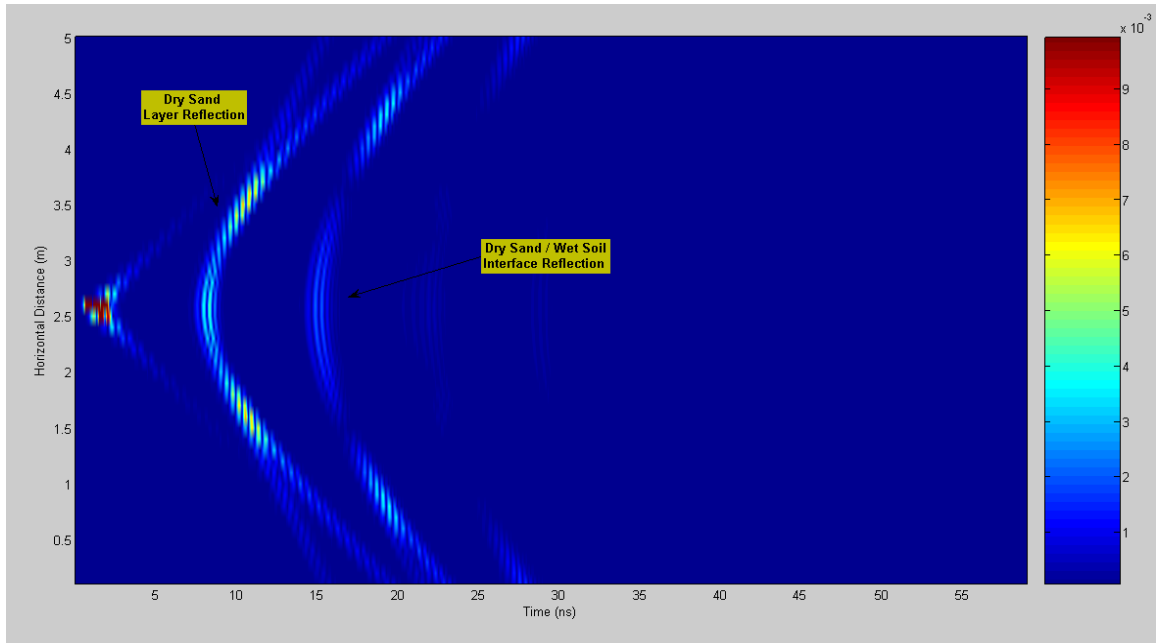


Figure 5.18: The simulation results in CMP configuration with 40 cm wet soil.

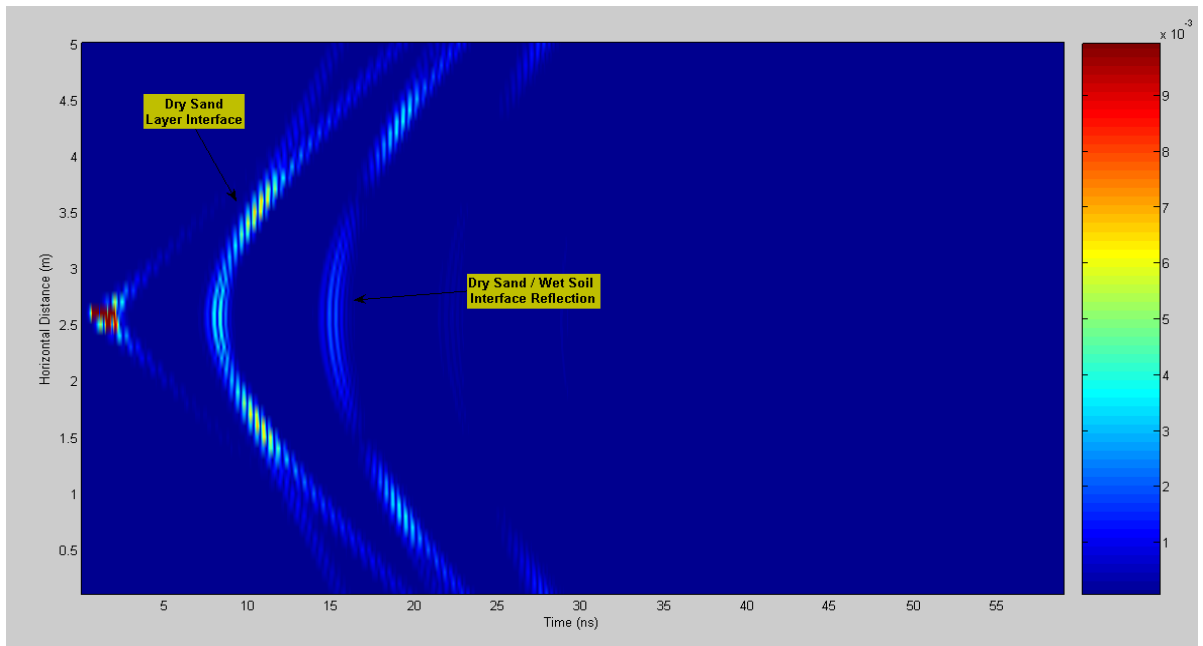


Figure 5.19: The simulation results in CMP configuration with 60 cm wet soil.

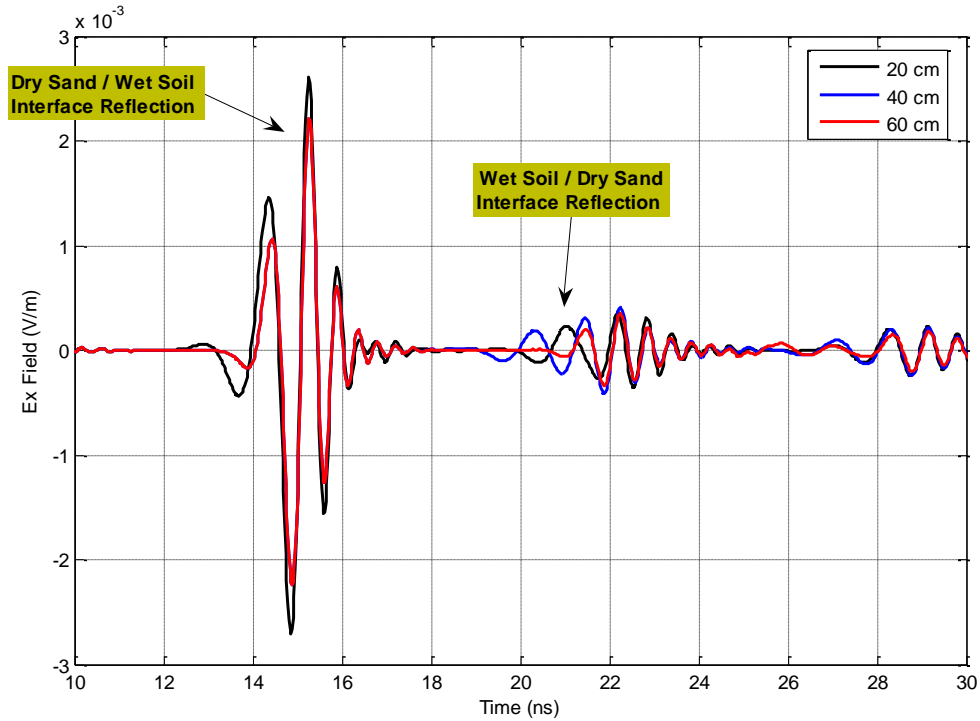


Figure 5.20: The simulation results from one receiver for 20, 40 and 60 cm layer.

The first thing to observe in these results is the tendency of the 20cm layer to reflect higher amplitude signal at the dry sand/wet soil interface due to its lower thickness. The same observation can be seen for the second reflection where 40 cm layer reflected a signal higher than 60 cm reflected signal. The 20 cm layer did not reflect higher signal amplitude (energy) than the other two layers in the second reflection since its transmitted signal in the first interface has lower amplitude (energy) than the transmitted signals of the other two layers. Another observation also, is the smoother transition of the 20cm reflection signal from zero state to its peak, compared to the other layers reflections, which suggests that at this short interval 20cm signal has low frequency band compared to the other two. This also applies to the 20cm and 40cm signals in the second reflection.

### 5.2.5 Third Case: Simulation of Localized Wet Soil

In this case, we simulate a system composed of two layers air and non-dispersive dry sand. In the second layer, localized dispersive wet soil was located at two different locations (see Figure 5.21). The simulations were carried out two times where each time the wet soil location was changed. The dispersive soil dimension was one by one meter. The main objective of this scenario is to test the ability of the GPR signal to detect and locate the dispersive wet soil such as the case of water leakage. The simulation results of both cases are shown in Figure 5.22 and Figure 5.23. In both cases, the GPR was able to detect the dispersive soil. However, the results reveal that the receiver location is a critical factor in the detection of these localized wet soils. Only those receivers, which were directly above the wet soil, were able to detect the reflected signal (see Figure 5.24). Location might be approximated through the distance between the receivers, which detect the reflected signals and the GPR transmitter.

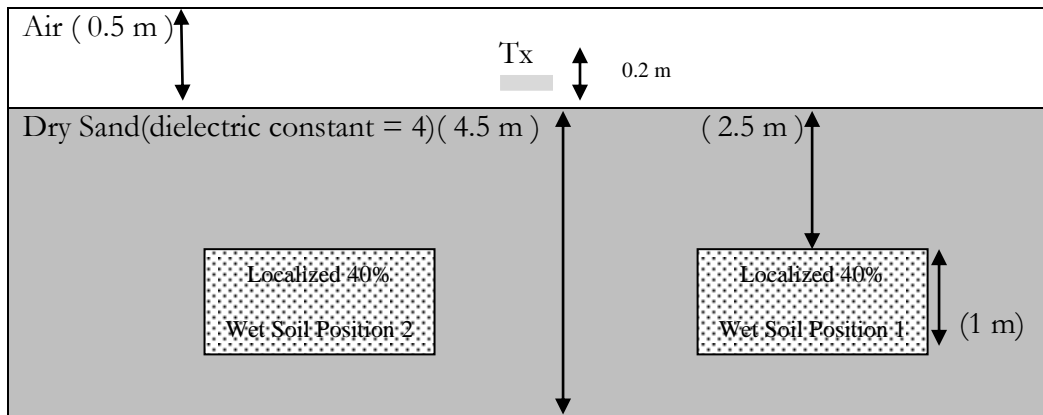


Figure 5.21: The simulation domain for the third case.



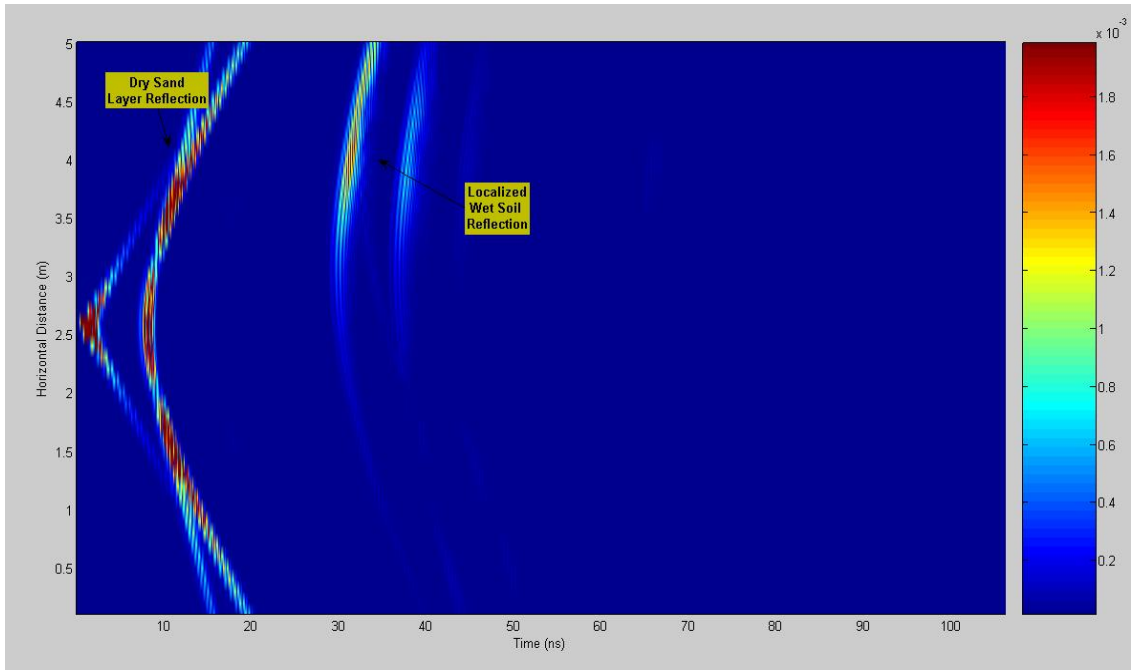


Figure 5.22: The simulation results in CMP configuration for Localized 40 % wet soil at position 1.

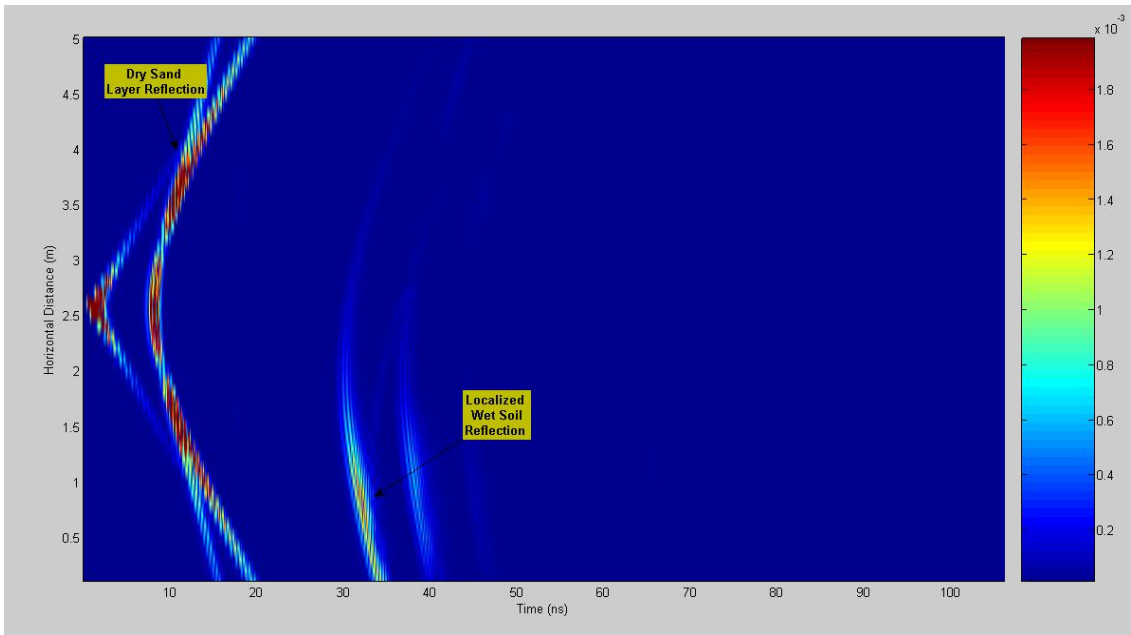


Figure 5.23: The simulation results in CMP configuration for Localized 40 % Wet Soil at position 2.

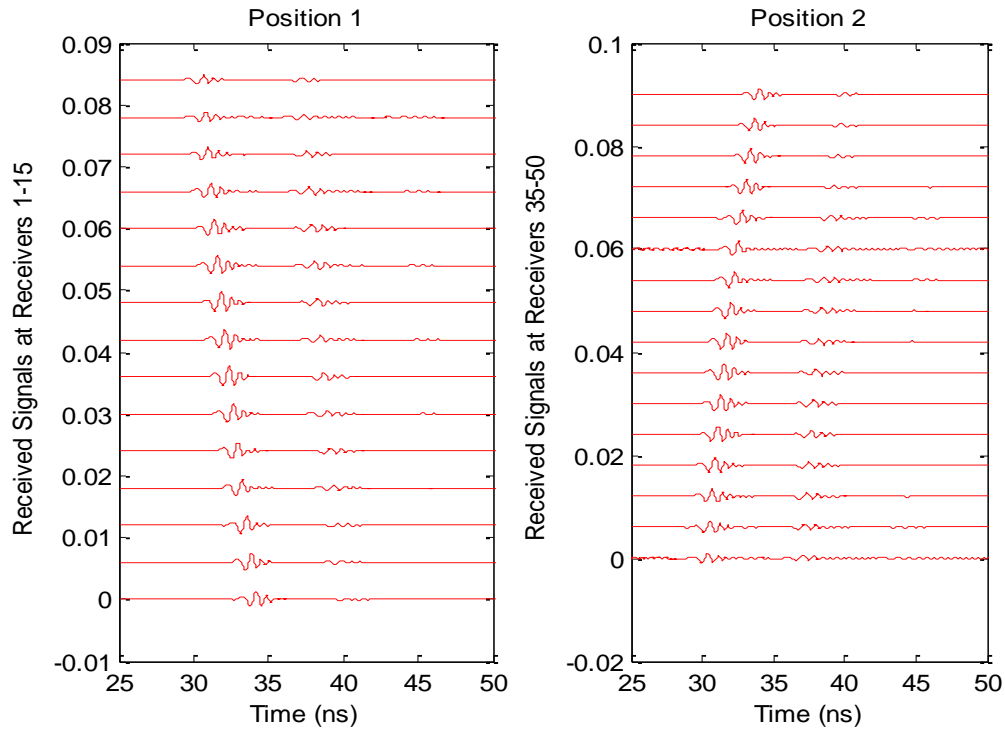


Figure 5.24: Time profile of the received signals at different receiver locations for localized wet soil at position 1 and position 2.

### 5.2.6 Fourth Case: Simulation of Non-Metallic Pipe Leakage

In the fourth case, a practical problem is considered. A system composed of air and non-dispersive dry sand layer with 80 cm diameter non-metallic buried pipe was simulated. The pipe is assumed to be Polyvinyl Chloride (PVC) pipe filled with non-dispersive water. The pipe outer diameter is 82 cm with 2 cm wall thickness. The simulations were carried out four times. In the first time GPR signal was transmitted through the mentioned system. The main goal of the first case is to identify the water pipe reflected signal. In the remaining three cases, the pipe is assumed to be defective and water leakage with 40%, 30% and 20% moisture level were assumed to appear below it. The

dimension of the wet soil was half a meter by two meters. Figure 5.25 show the simulated system configuration.

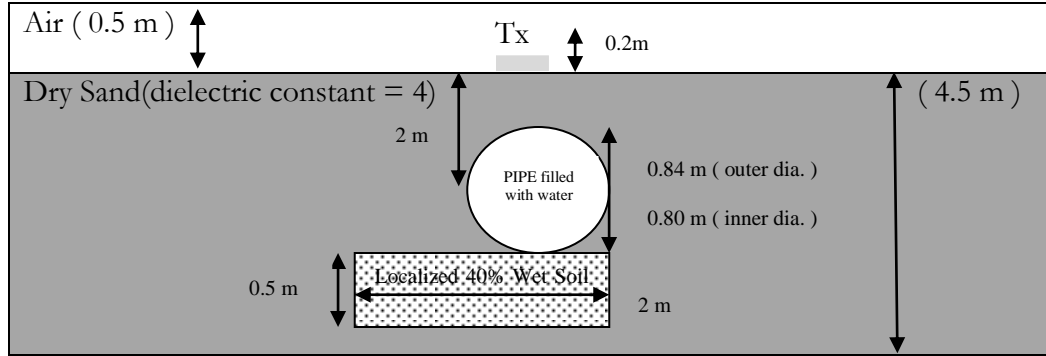


Figure 5.25: The simulation domain for the fourth case.

Figure 5.26 shows the simulation results of the first case. The water pipe top and bottom side reflection is clear at the central receivers. Figures 5.27, 5.28 and 5.29 show the simulation results for cases 2 to 4 with 40%, 30% and 20% moisture level, respectively. In each case, the leakage was detected. However, since this leakage is localized, the receiver location plays an important role in the leakage detection. Figure 5.30 shows receiver at horizontal position five received signals. Sharp signal reflection can be noticed for 40% and 30% with respect to 20% reflection. This suggests higher frequency contents for these two signals with respect to 20% signal. Also, as noticed in the first two layers case, due to higher permittivity higher reflection was noticed for 40% wet soil compared to the other two soil cases.

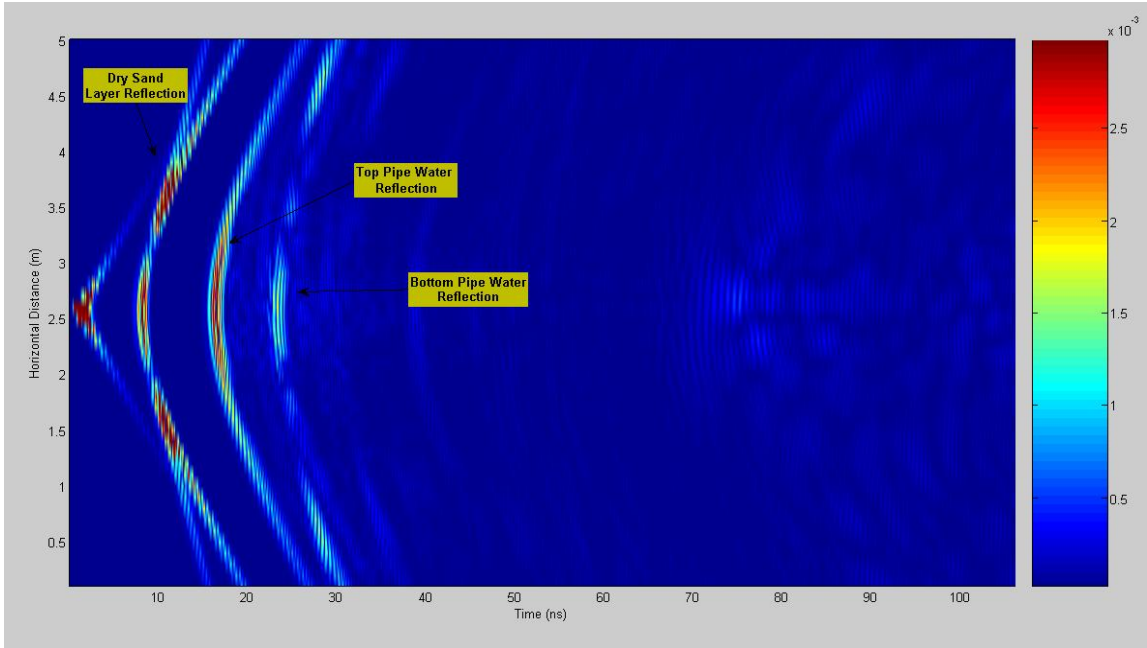


Figure 5.26: The simulation results in CMP configuration for pipe without leakage.

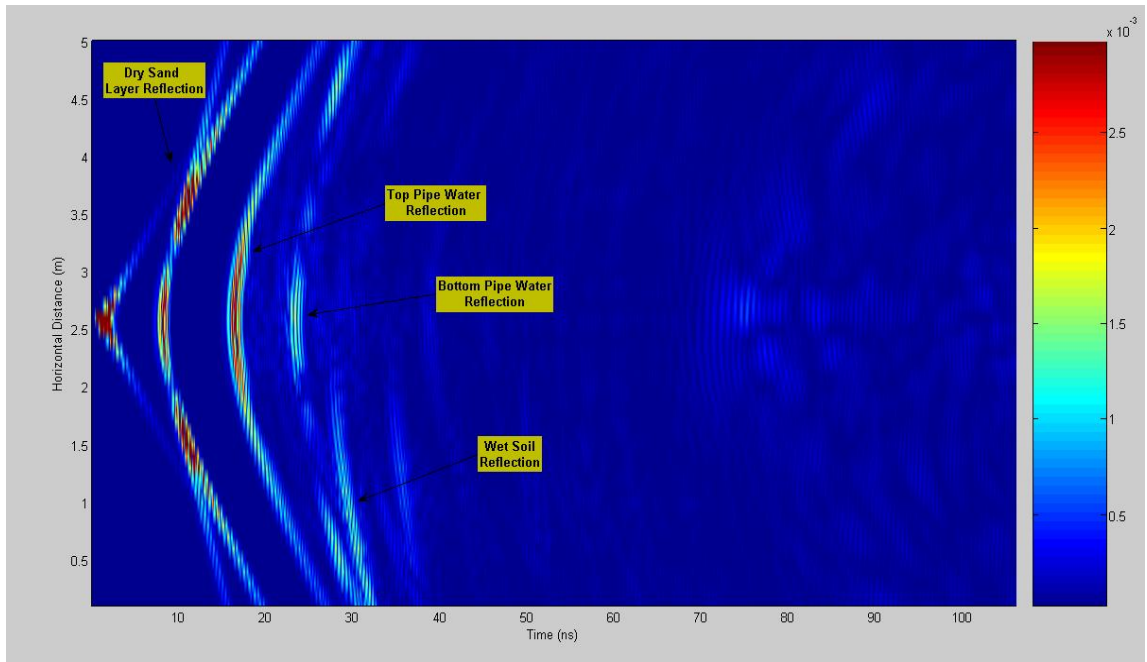


Figure 5.27: The simulation results in CMP configuration for pipe leakage with localized 40% wet soil.

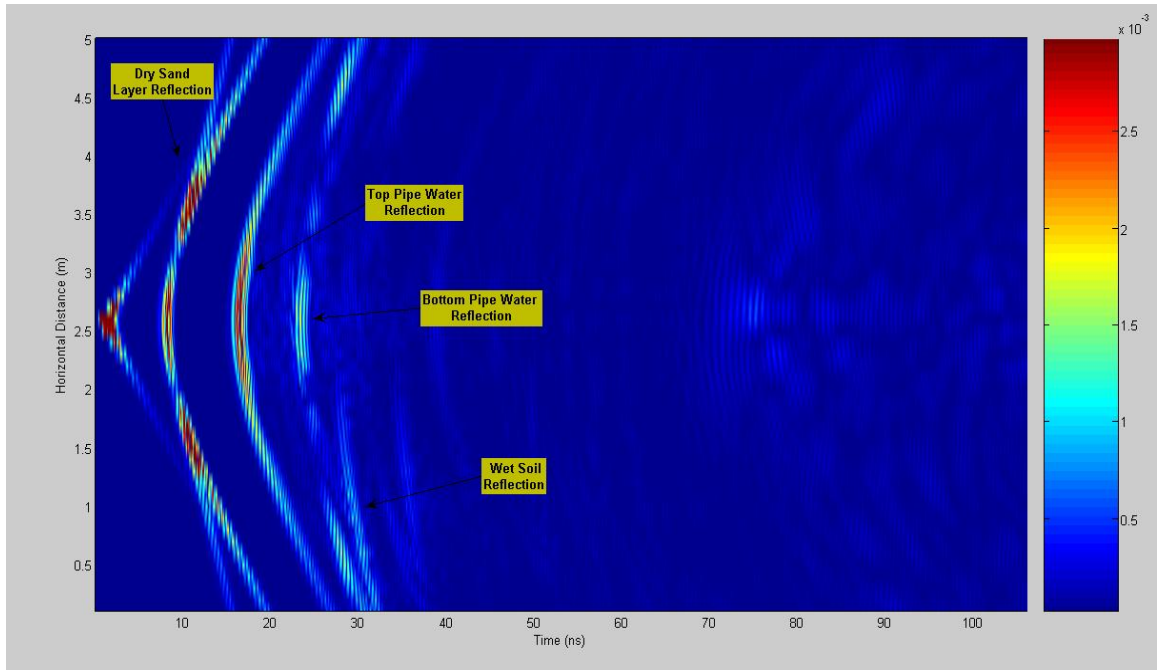


Figure 5.28: The simulation results in CMP configuration for pipe leakage with localized 30% wet soil.

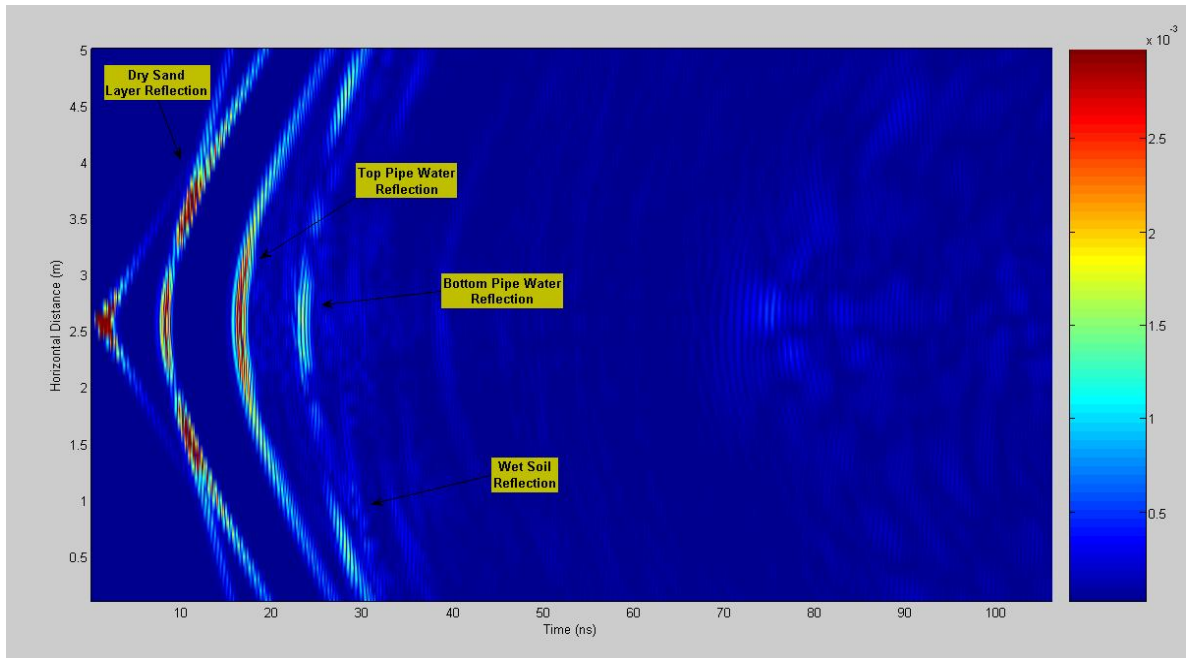


Figure 5.29: The simulation results in CMP configuration for pipe leakage with localized 20% wet soil.

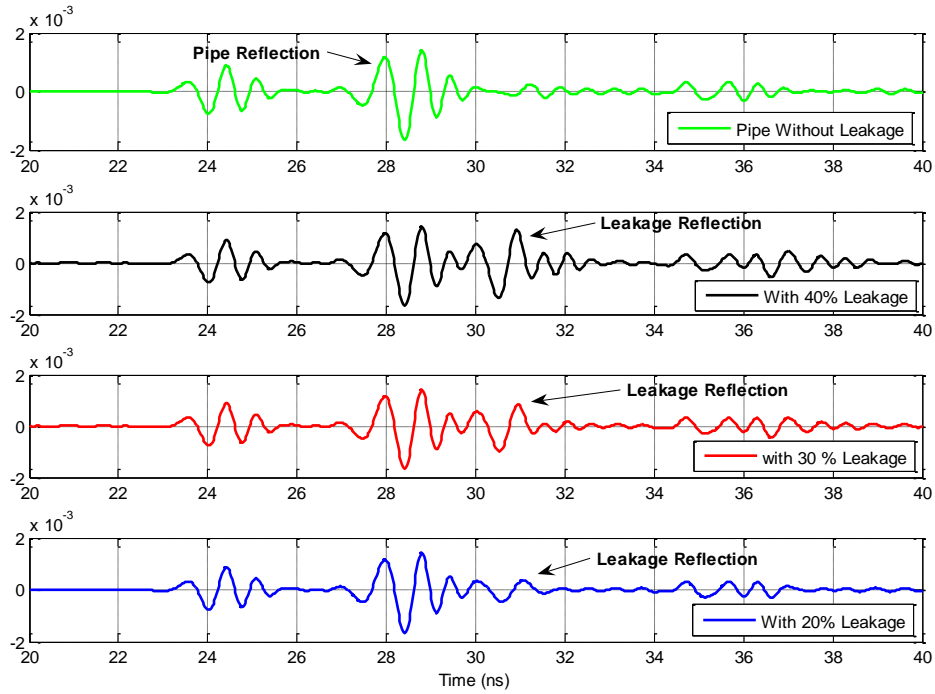


Figure 5.30: The simulation results from receiver number 5 for the fourth case simulation with different moisture levels.

### 5.2.7 Fifth Case: Simulation of Magnetic Dispersive Material

In the previous cases, only electrically dispersive material was considered. However, the proposed algorithm is capable of simulating GPR wave propagation in electric and magnetic dispersive materials. In this case, a hypothetical material with electric and magnetic dispersion properties modeled by a three-pole Debye model was assumed to be buried in dry sand (see Figure 5.31). Table 5.3 present Debye model parameters that were used and Figures 5.32 and 5.33 show the electric and magnetic dispersion relation of the modeled material, respectively.

Table 5.3: Multi-pole Debye selected parameters for the hypothetical material.

Dispersion Type	1st Pole	2nd Pole	3rd Pole
<i>Electric</i> $\epsilon_{inf}=15.271$	$\epsilon_s=24.835$	$\epsilon_s=16.75$	$\epsilon_s=2.206 \times 10^{-4}$
	$\epsilon_{\infty}=15.271$	$\epsilon_{\infty}=15.271$	$\epsilon_{\infty}=1$
	$\omega_o=1$	$\omega_o=1$	$\omega_o=1$
	$\delta=1.042 \times 10^{-10}$	$\delta=3.168 \times 10^{-9}$	$\delta=8.854 \times 10^{-12}$
	$d=0$	$d=0$	$d=0$
<i>Magnetic</i> $\epsilon_{inf}=29.3$	$\mu_s=30.227$	$\mu_s=6$	$\mu_s=7$
	$\mu_{\infty}=1$	$\mu_{\infty}=1$	$\mu_{\infty}=1$
	$\omega_o=1$	$\omega_o=1$	$\omega_o=1$
	$\delta=1.149 \times 10^{-10}$	$\delta=2.364 \times 10^{-11}$	$\delta=2.532 \times 10^{-12}$
	$d=0$	$d=0$	$d=0$

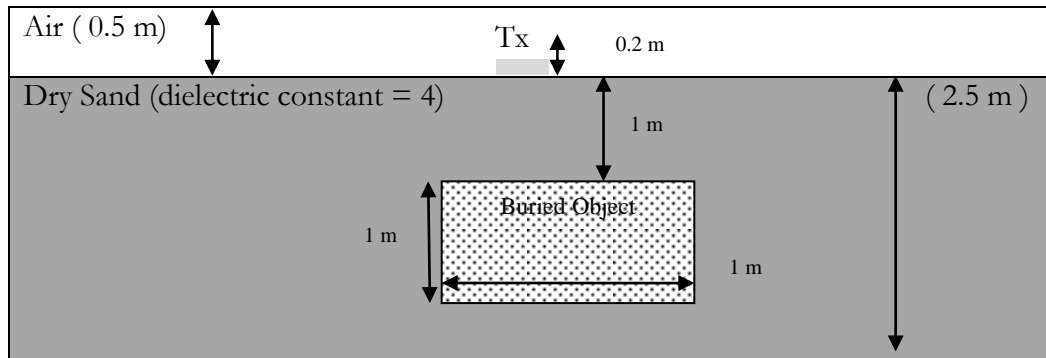


Figure 5.31: The simulation domain for the fifth case.

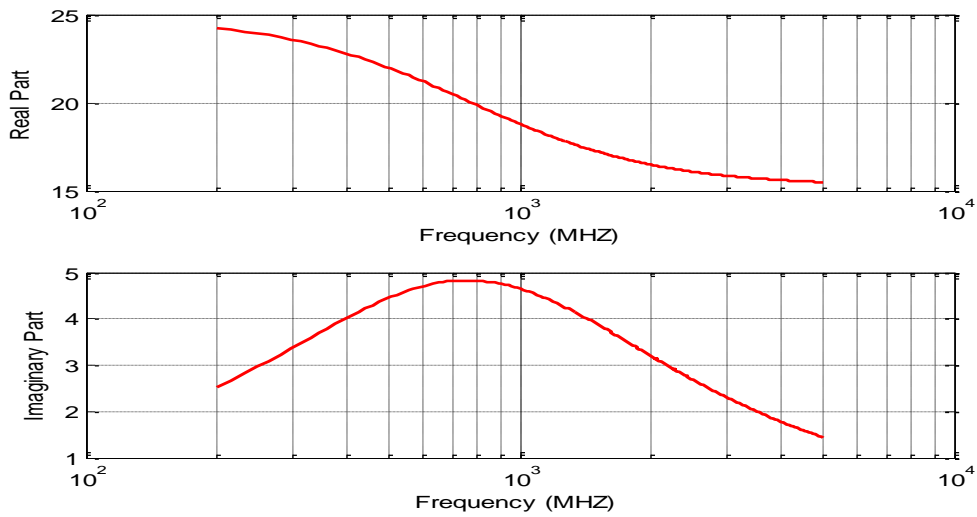


Figure 5.32: Real and imaginary permittivity for the hypothetical material.

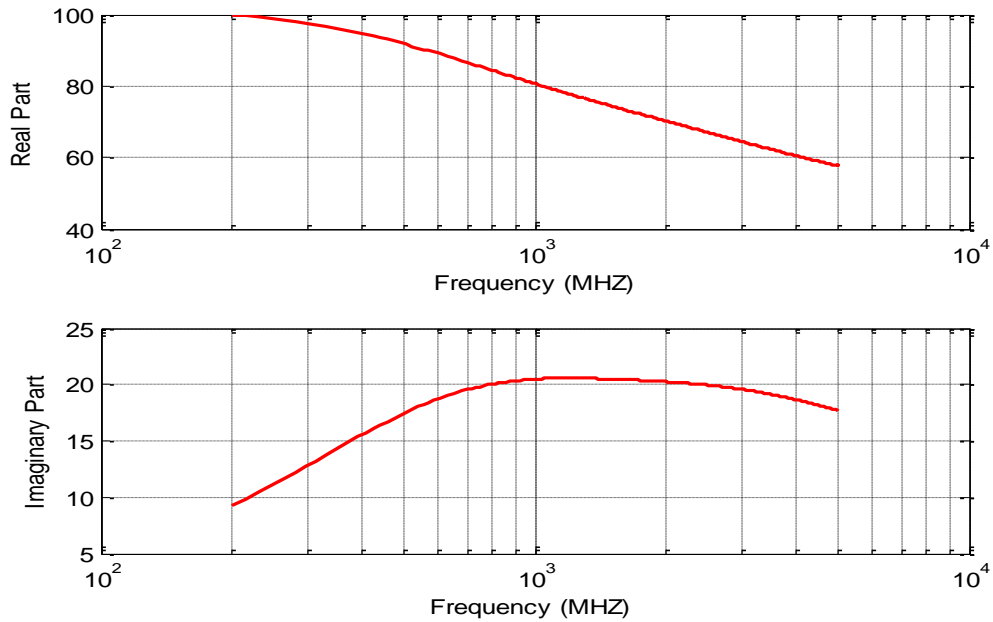


Figure 5.33: Real and imaginary permeability for the hypothetical material.

The simulations were carried out four times. The first time only static permittivity and permeability are considered (non-dispersive system). The second time only magnetic dispersion is considered while the third time only electric dispersion is considered. The fourth system includes both electric and magnetic dispersion. Figure 5.34 shows the simulation results for all cases. Comparing the last three cases it can be seen that the electric dispersion has stronger influence in the reflected signal and can minimize the magnetic dispersion features when both are present. Also, as in the previous cases, considering the dispersion properties (either electric or magnetic) minimizes the overall reflected signal energy.



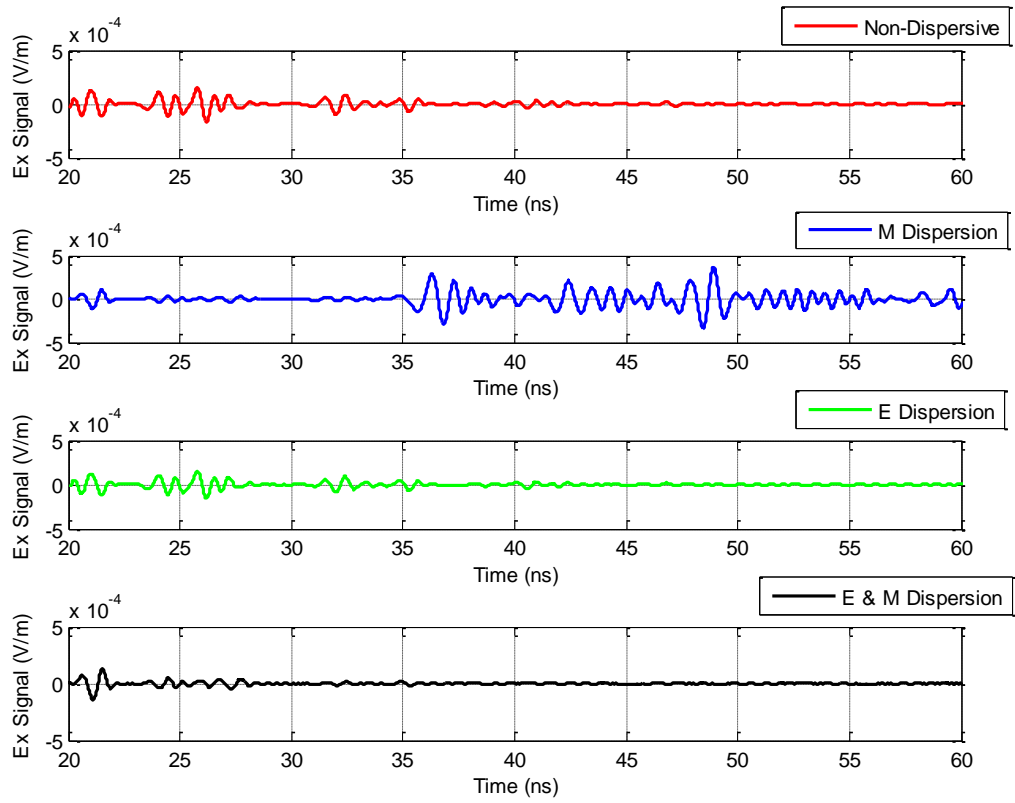


Figure 5.34: The simulation results for the fifth case.

## **6 TIME-FREQUENCY ANALYSIS OF THE SIMULATED CASES**

A study of the received signal characteristics versus the change in material properties is possible. Distinct material signatures and features can be extracted from the generated synthetic data by proper signal processing. In this chapter, time-frequency analysis for some of the simulated cases will be presented.

### **6.1 Conventional Characteristic Features**

A feature is a unique characteristic of a signal that alters an original data, however it keep vital information of the data stream. It can affect a data stream with different effects. For example, it can cause reduction in pulse rise time, pulse spreading, change the arrival time of a particular mode or shifting a dispersion curve. There are two main features generally, time-domain and frequency domain features [59].

GPR reflected signals composed of many reflections from different discontinuities which appear in the received signal stream as an abrupt time limited changes which suggest that its FT contains time varying spectral characteristics. Hence, the conventional Fourier decomposition is not a suitable tool for analyzing these signals, as it assume that the signal sinusoidal representation extent over the whole signal time domain.

To overcome this problem the Discrete Time-Frequency technique shall be used for GPR signal analysis. This technique has been used successfully for features extraction of ultrasonic defect classification signal[59], which has close reflection behavior to GPR signals .

## 6.2 Time-Frequency

The main principle of the discrete time frequency analysis is to divide discrete time domain signal into many sub-signals in the time domain then perform discrete FT for each sub-signal. This way the frequency contents will be strongly dependent of the time domain. Basically, TF analysis can be implemented by applying window function with short time duration to the discrete time domain signal then FT the resulted signal. This can be represented mathematically with Equation 6.1.

$$F(n, f) = \sum_{n=-\infty}^{n=\infty} f[n]w[n - m]e^{-j2\pi fn} \quad (6.1)$$

For the remaining of this chapter, we will present TF analysis for the recorded GPR signals in the preliminary case, first case and the fourth case (refer to Chapter 5). Note that for each TF figure, dark red color represents highest amplitude and dark blue represent lowest amplitude.

### 6.2.1 TF Analysis for the Preliminary Case:

The recorded signals for the preliminary case are presented in Figure 6.1. The TF analysis for these two signals are presented in figure 6.2. As it can be seen from the TF analysis, at the time of interest (5 to 10 ns) the non-dispersive signal has higher frequency components compared to the dispersive case. This can be interpreted in the time domain signal (Figure 6.1) by the smoother wave transition of the dispersive signal compared to the sharper transition for the non-dispersive signal.

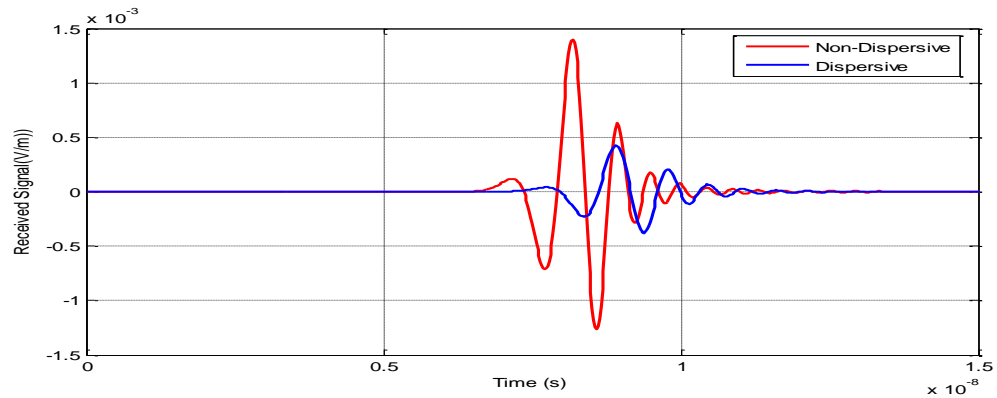


Figure 6.1: Time profile of the received signal with (blue) and without (red) consideration of the material dispersion.

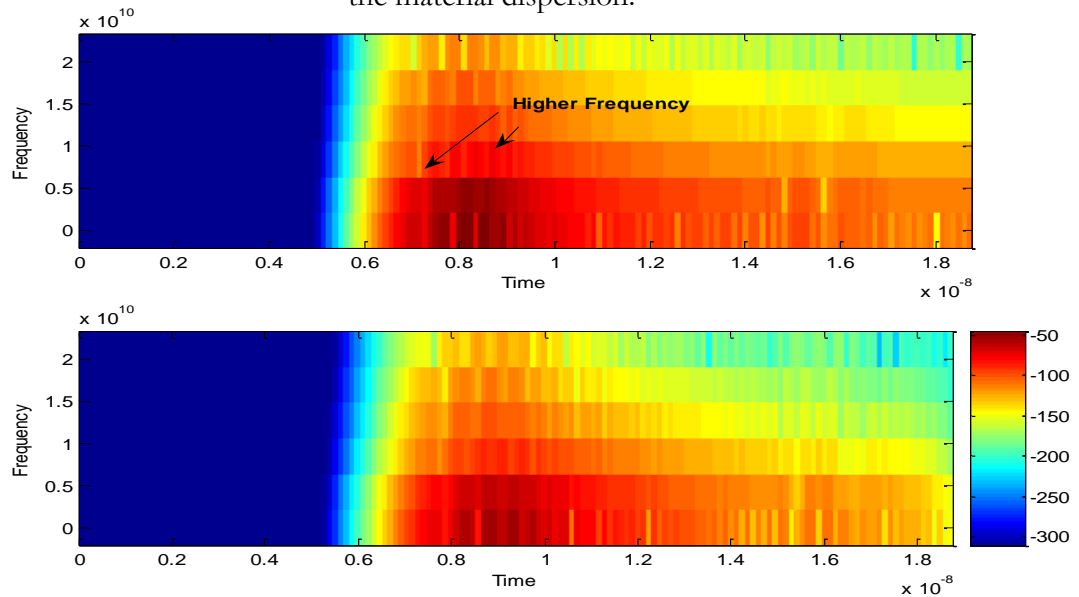


Figure 6.2: Time – Frequency analysis of the recorded signal for non-dispersive (Top) and dispersive (bottom) for the preliminary case.

### 6.2.2 TF Analysis for the First Case:

The recorded signals for the first case is presented in figure 6.3. The TF analysis for these signals is presented in Figure 6.4 and Figure 6.5. As it can be seen from the TF analysis, at the time of interest (5 to 10 ns) the red color width is higher for higher moisture signals which suggests higher frequency components compared to the lower ones. This can be interpreted in the time domain signal by the relatively sharper wave transition of the higher moisture level signals compared to the smoother transition for the lower moisture level signals.

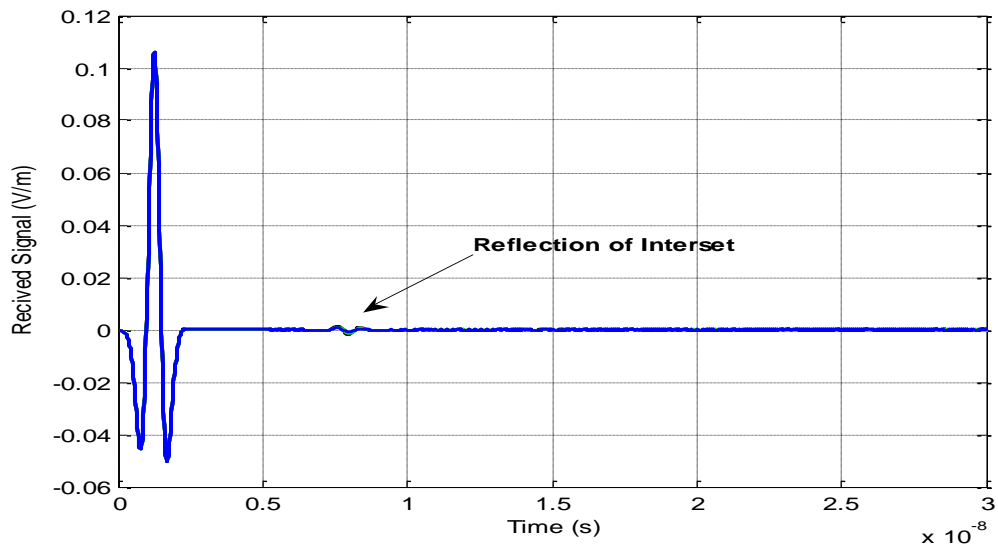


Figure 6.3: Time profile of the received signals for the first case.

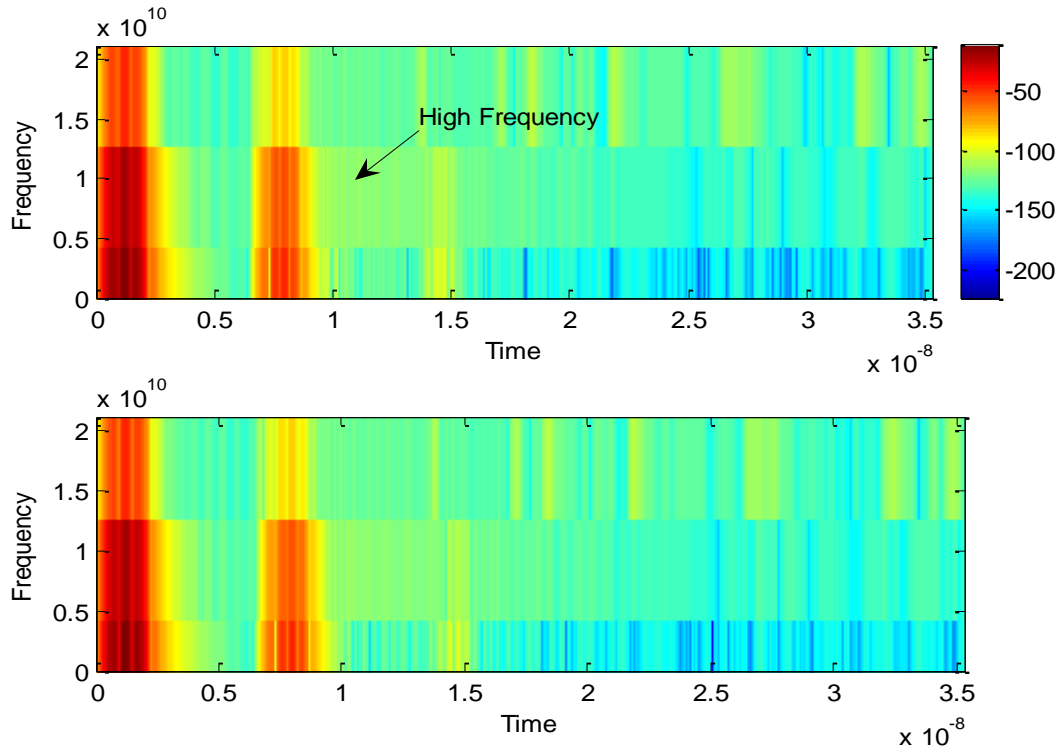


Figure 6.4: Time – Frequency analysis of the recorded signal for 40% case (Top) and 30% case (bottom) for the first case.

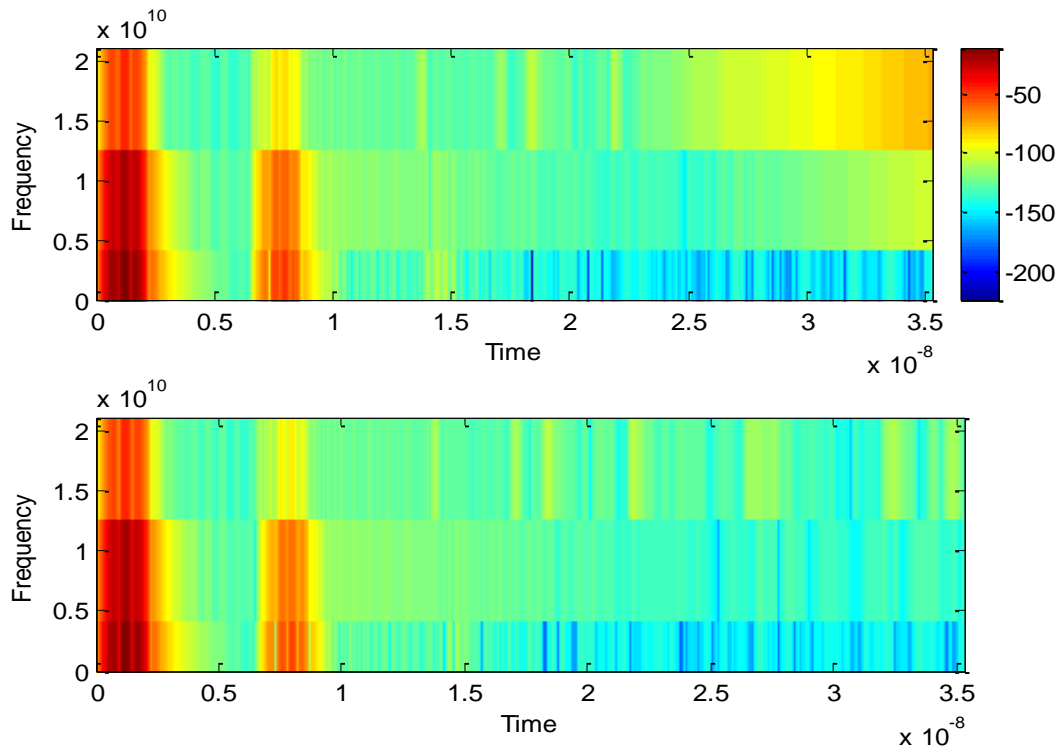


Figure 6.5: Time – Frequency analysis of the recorded signal for 20% case (Top) and 10% case (bottom) for the first case.

### 6.2.3 TF Analysis for the Fourth Case:

The recorded signals for the fourth case is presented in figure 6.6. The TF analysis for these signals is presented in Figures 6.7 and Figure 6.8. At the time of interest (20 to 40 ns) leakage can be identified around 30 ns. Also, signal reflection close to 40 ns can characterize the moisture level since it give distinct signal amplitude to each level. This may help in the usage of this analysis in the identification of the soil moisture level in general.

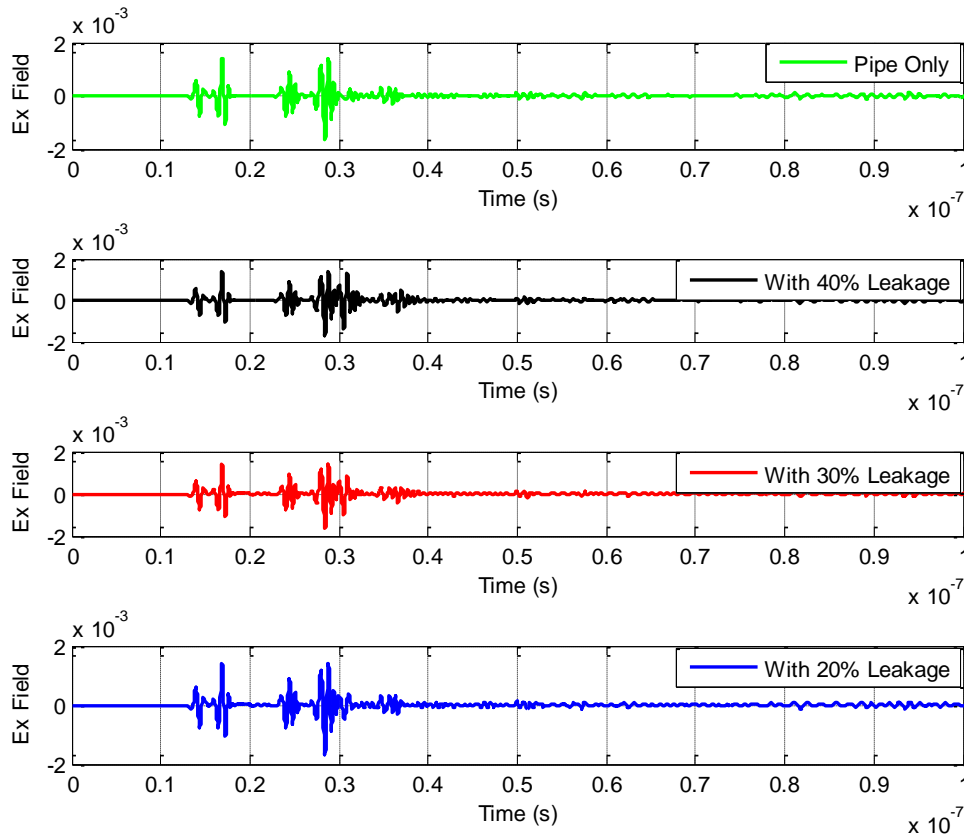


Figure 6.6: Time profile of the received signals for the fourth case.

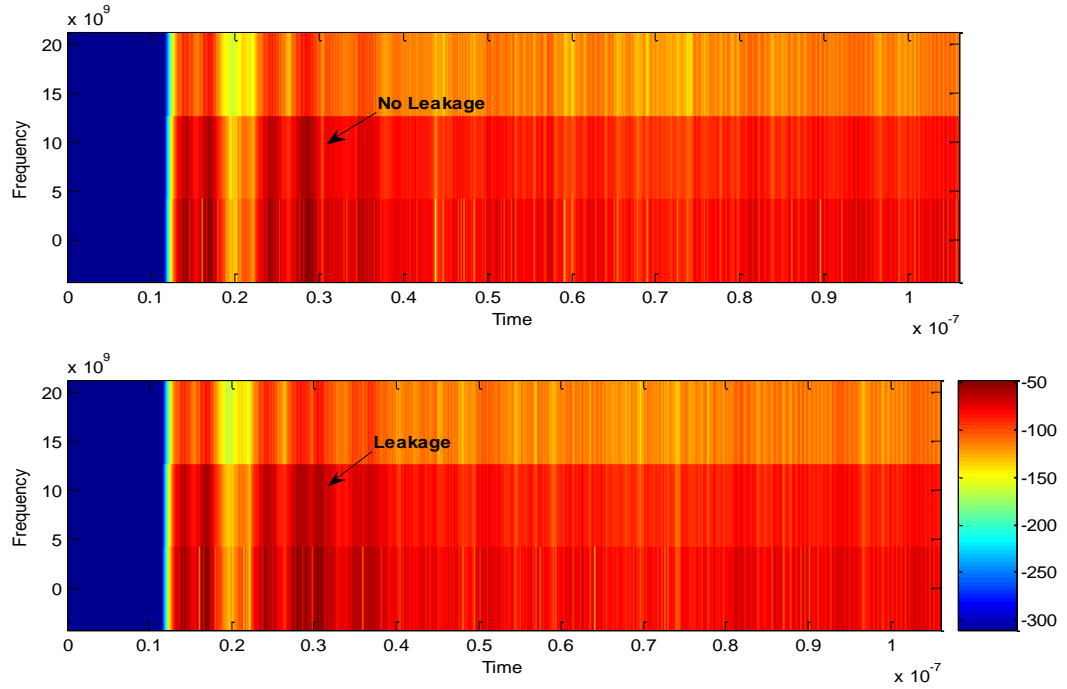


Figure 6.7: Time – Frequency analysis of the recorded signal for Pipe only (Top) and Pipe with 40%leakage (bottom) for the fourth case.

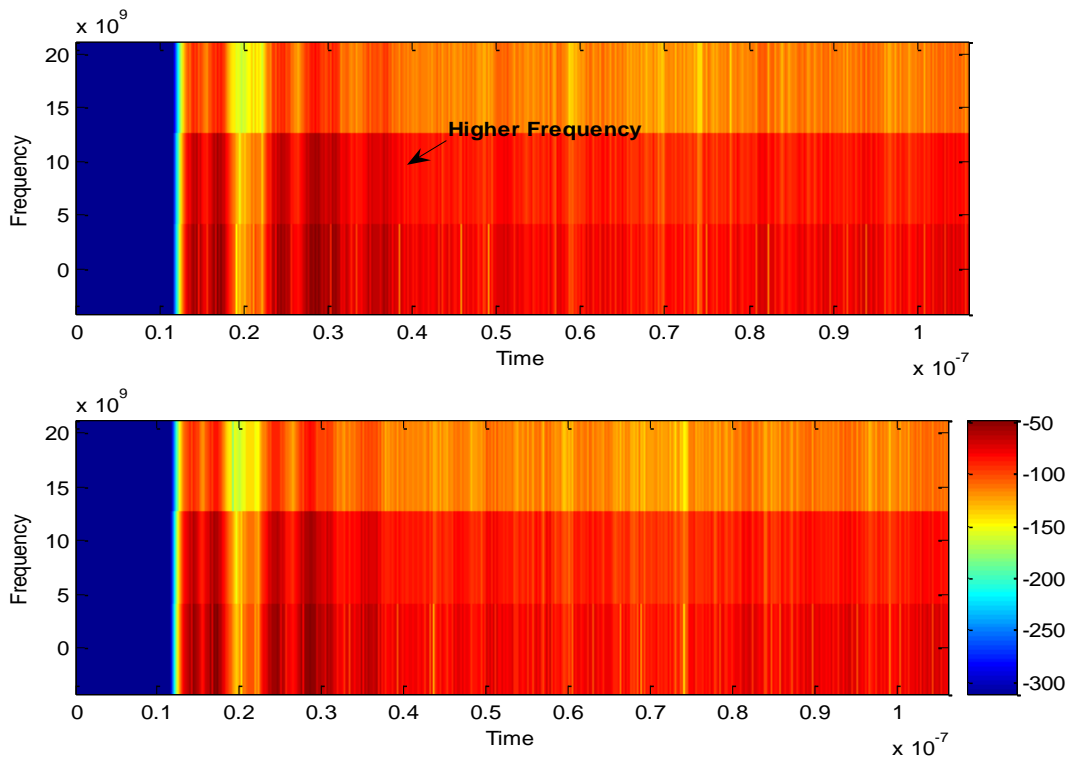


Figure 6.8: Time – Frequency analysis of the recorded signal for Pipe with 30%leakage (Top) and Pipe with 20%leakage (bottom) for the fourth case.



## CONCLUSIONS AND RECOMMENDATIONS

### Summary and Conclusions

In this research, an advanced GPR simulation system was developed using a new general polarization FDTD-ADE algorithm. The developed algorithm is stable and capable of simulating two and three dimensional GPR signal propagation through lossy, electric and/or magnetic dispersive or totally non-dispersive materials. This algorithm can be used with different multi-pole electric and magnetic dispersion models. The proposed algorithm was validated against previously developed algorithms and analytical solutions with excellent agreement.

FORTTRAN programming language was used to implement the developed algorithm. The developed simulator was used to simulate different cases with different electric and magnetic dispersive systems. Recent advanced dispersion model for wet soil was fitted to five-pole Lorentz dispersion model and used in most of the simulated cases. Simulation results were presented in CMP configuration. The developed simulator shows ability to detect localized wet dispersive soil in dry sand and to detect water leakage from buried non-metallic pipe. The simulator also was sensitive and gave distinct output for different soil moisture percentage. Detection of buried three-pole magnetically dispersive material was achieved successfully with the proposed algorithm.

## **Recommendation for Future Research**

For further research, we recommend extensions along the following directions:

1. The algorithm can be developed to be used with other EM waves at different bandwidths once non-linear polarization models were included.
2. Different antenna models shall be included to be used with this algorithm to provide results that are more realistic.
3. Magnetic dispersion relations of different ground materials shall be studied and reported to be used in such simulator.
4. Further signal processing tools can be used to manipulate the received signals and provide characteristic features for each moisture percentage.

# References

- [1] D.J. Daniels, **Ground Penetrating Radar** - 2nd edition, *IEEE*, London, 2004.
- [2] Samer Lahouar, and Imad L. Al-Qadi "**Automatic detection of multiple pavement layers from GPR data**" *NDT & E International* ,vol 41, Issue 2, March 2008, Pages 69-81
- [3] M R Shaw, S G Millard, T C K Molyneaux,,J H Bungey, M J Taylor " **Location of Steel Reinforcement in Concrete using Ground Penetrating Radar**" *NDT & E International*, vol 38, Issue 3, April 2005, Pages 203-212
- [4] David Lopes de Castro, and Raimundo Mariano Gomes CasteloBranco "**4-D ground penetrating radar monitoring of a hydrocarbon leakage site in Fortaleza (Brazil) during its remediation process: a case history**" *Journal of Applied Geophysics*,vol 54, Issues 1-2, November 2003, Pages 127-144
- [5] L. Crocco, G. Prisco, F. Soldovieri and N.J. Cassidy."**Early-stage leaking pipes GPR monitoring via microwave tomographic inversion** ". *Journal of Applied Geophysics*, vol 67, Issue 4, April 2009, Pages 270-277
- [6] N. S. Duxbury ,S. S. Abyzov, V. E. Romanovsky and K. Yoshikawa " **A combination of radar and thermal approaches to search for methane clathrate in the Martian subsurface** " *Planetary and Space Science*, vol 52, Issues 1-3, January-March 2004, Pages 109-115
- [7] FaezehSh.A. Ghasemi and M.S. Abrishamian."**A novel method for FDTD numerical GPR imaging of arbitrary shapes based on Fourier transform**". *NDT & E International*.vol 40, Issue 2, March 2007, Pages 140-146
- [8] Huisman, J.A., Hubbard, S.S., Redman, J.D., Annan, A.P., 2003."**Measuring soil water content with ground penetrating radar: a review**".*Vadose Zone* 2, 476–491.
- [9] Topp, G.C., Davis, J.L., Annan, A.P., 1980. "**Electromagnetic determination of soil water content: measurements in coaxial transmission lines**". *Water Resource Research* 16, 574–582.

- [10] Herkelrath, W.N., Hamburg, S.P., Murphy, F., 1991. "**Automatic, realtime monitoring of soil moisture in a remote field area with time domain reflectometry**". *Water Resource Research* 26, 2311–2316.
- [11] Hubbard, S.S., Peterson Jr., J.E., Majer, E.L., Zawislanski, P.T., Williams, K.H., Roberts, J., Wobber, F., 1997. "**Estimation of permeable pathways and water content using tomographic radar data**". *The Leading Edge* 16, 1623–1630.
- [12] Alumbaugh, D., Chang, P.Y., Paprocki, L., Brainard, J.R., Glass, R.J., Rautman, C.A., 2002. "**Estimating moisture contents in the vadose zone using cross-borehole ground penetrating radar: a study of accuracy and repeatability**". *Water Resource Research* 38 (12), 1309.
- [13] Grote, K., Hubbard, S.S., Rubin, Y., 2003. "**Field-scale estimation of volumetric water content using GPR ground wave techniques**". *Water Resource Research* 39 (11), 1321.10.1029/2003WR002045.
- [14] Huisman, J.A., Sperl, C., Bouten, W., Verstraten, J.M., 2001. "**Soil water content measurements at different scales: accuracy of time domain reflectometry and ground-penetrating radar**". *Journal of Hydrology* 254 (1–2), 48–58.
- [15] Baker, G.S., 1998. "**Applying AVO analysis to GPR data**". *Geophysical Research Letters* 25 (3), 397–400.
- [16] Greaves, R.J., Lesmes, D.P., Lee, J.M., Toksoz, M.N., 1996. "**Velocity variations and water content estimated from multi-offset, ground-penetrating radar**". *Geophysics* 61, 683–695.
- [17] Tillard, S., Dubois, J.-C., 1995. "**Analysis of GPR data: wave propagation velocity determination**". *Journal of Applied Geophysics* 33, 77–91.
- [18] Ulrikson, C.P.F., 1982. "**Application of impulse radar to civil engineering**". PhD thesis, Lund University of Technology, Sweden.
- [19] Grote, K., Hubbard, S.S., Rubin, Y., 2002. "**GPR monitoring of volumetric water content in soils applied to highway construction and maintenance**". *The Leading Edge* 21, 482–485.
- [20] Stoffregen, H., Zenker, T., Wessolek, G., 2002. "**Accuracy of soil water content measurements using ground penetrating radar: comparison of ground penetrating radar and lysimeter data**". *Journal of Hydrology* 267, 201–206.

- [21] Jeffrey J. Daniels, Roger Roberts, Mark Vendl 1995. "**Ground penetrating radar for the detection of liquid contaminants**". *Journal of Applied Geophysics* 33 , 195-207
- [22] Goodman, D., 1994. "**Ground-penetrating radar simulation in engineering and archeology**". *Geophysics* 59, 224–232.
- [23] Zeng, X., McMechan, G.A., Cai, J., Chen, H.W., 1995. "**Comparison of ray and Fourier methods for modeling monostatic ground-penetrating radar profiles**". *Geophysics* 60, 1727–1734.
- [24] Ellefsen, K.J., 1999. "**Effects of layered sediments on the guided wave in crosswell radar data**". *Geophysics* 64, 1698–1707.
- [25] Lui, Q.H., Fan, G., 1999. "**Simulations of GPR in dispersive media using a frequency-dependent PSTD algorithm**". *IEEE Transactions on Geoscience and Remote Sensing* 37, 2317–2324.
- [26] J. M. Bourgeois and G. S. Smith, "**A fully three-dimensional simulation of a ground-penetrating radar: FDTD theory compared with experiment**". *IEEE Trans. Geosci. Remote Sensing*, vol. 34, pp. 36–44, Jan.1996.
- [27] U. Oğuz and L. Gürel, "**Subsurface-scattering calculations via the 3DFDTD method employing PML ABC for layered media**". *IEEE Antennas Propagation Soc. Int. Symp. URSI Radio Science Meeting*, Montréal, QC, Canada, July 1997.
- [28] L. Gürel and U. Oğuz, "**Three-dimensional FDTD modeling of a ground penetrating radar**". *IEEE Trans. Geosci. Remote Sensing*, vol. 38, pp. 1513–1521, July 2000.
- [29] D. Sullivan, "**Frequency-Dependent FDTD Method Using Z-Transform**". *IEEE Transactions on Antennas & Propagation* 40, 1223-1230 (1992).
- [30] Gürel, L. and U. Oğuz, "**Simulations of ground penetrating radars over lossy and heterogeneous grounds**". *IEEE Trans. Geosci. Remote Sensing*, Vol. 39, 1190-1197, June 2001.
- [31] Oğuz, U. and L. Gürel, "**Frequency responses of ground penetrating radars operating over highly lossy grounds**". *IEEE Trans. Geosci. Remote Sensing*, vol. 40, 1385-1394, June 2002.

- [32] Teixeira, F. L., W. C. Chew, M. Straka, M. L. Oristaglio, and T. Wang, "**Finite-difference time domain simulation of ground penetrating radar on dispersive, Inhomogeneous, and conductive soils**". *IEEE trans. Geosci. Remote Sensing*, vol. 36, 1928-1937, Nov. 1998.
- [33] Kane Yee (1966). "**Numerical solution of initial boundary value problems involving Maxwell's equations in isotropic media**". *IEEE Transactions on Antennas and Propagation* 14: 302–307
- [34] Sullivan DM. "**Electromagnetic simulation using the FDTD Method**". *IEEE Press*; 2000.
- [35] Taflove A, Hagness SC. "**Computational electrodynamics, the finite difference time domain method**". 2nd ed. Artech House Inc.; 2000.
- [36] Gurel L, Oguz U. "**Simulation of ground-penetrating radars over lossy and heterogeneous grounds**". *IEEE Trans Geosci Remote Sensing* 2001;30:1190–7.
- [37] J.P. Berenger, "**A perfectly matched layer for the absorption of electromagnetic waves**". *Jour. Comp. Phys.*, vol.114, Aug. 1994, pp.185-200.
- [38] Harry M. Jol, "**Ground Penetrating Radar: Theory and Applications**" *Elsevier*, 2009.
- [39] Fritzsche, M. 1995. "**Detection of buried landmines using ground penetrating radar**". *Proceedings of the SPIE* 2496 ,pp. 100-109.
- [40] Huisman, J.A., Hubbard, S.S., Redman, J.D., Annan, A.P., 2003. "**Measuring soil water content with ground penetrating radar: a review**". *Vadose Zone* 2, 476–491.
- [41] G. Klysz, and J.-P. Balayssaca "**Determination of volumetric water content of concrete using ground-penetrating radar**" *Cement and Concrete Research*. vol 37, Issue 8, August 2007, Pages 1164-1171
- [42] David Cist, Alan Schutz "**A Low-Cost GPR Gas Pipe & Leak Detector**" *Technical Report by Geophysical Survey Systems, Inc.* 13 Klein Drive N. Salem, NH 03073 submitted to US Dept. of Energy NETL 30 March 2005.
- [43] Dobson, M.C., F.T. Ulaby, M.T. Hallikainen, and M.A. El-Rayes. 1985. "**Microwave dielectric behavior of wet soil: II. Dielectric mixing models**". *IEEE Trans. Geosci. Remote Sens.* 23:35–46.

- [44] Roth, K., R. Schulin, H. Flüßler, and W. Attinger.1990. "**Calibration of time domain reflectometry for water content measurements using a composite dielectric approach**". *Water Resour. Res.* 26:2267–2273.
- [45] Dirksen, C., and S. Dasberg. 1993. "**Improved calibration of time domain reflectometry soil water measurements**". *Soil Sci. Soc. Am. J.* 57:660–667.
- [46] Heimovaara, T.J., W. Bouten, and J.M. Verstraten. 1994. "**Frequency domain analysis of time domain reflectometry waveforms: 2. A four-component complex dielectric mixing model for soils**". *Water Resour. Res.* 30:201–209.
- [47] Or, D., and J.M. Wraith. 1999. "**Temperature effects on soil bulk dielectric permittivity measured by time domain reflectometry: A physical model**". *Water Resources. Res.* 35:371:383.
- [48] Boyarskii, D.A., V.V. Tikhonov, and N.Yu.Komarova.2002. "**Model of dielectric constant of bound water in soil for applications of microwave remote sensing**". *Journal of Electromagnetic Waves Appl.* 16:411–412.
- [49] Mironov, V.L., M.C. Dobson, V.H. Kaupp, S.A. Komarov, and V.N. Kleshchenko. 2004. "**Generalized refractive mixing dielectric model for moist soils**". *IEEE Trans. Geosci. Remote Sens.* 42:773–785.
- [50] Schwartz, R. C., S. R. Evett, and J. M. Bell, "**Complex permittivity model for time domain reflectometry soil water content sensing: I. Theory**" *Soil Sci. Soc. Am. J.*, vol. 73, 886-897, 2009.
- [51] Birchak, J.R., C.G. Gardner, J.E. Hipp, and J.M. Victor.1974. "**High dielectric constant microwave probe for sensing soil moisture**". *Proc. IEEE* 62:93–98.
- [52] A. P. Zhao, A. Renko and M.A Rinne, "**Material independent PML absorbers for arbitrary anisotropic dielectric media**".*Electronics Letters*, vol. 33, pp. 1535-1536, 1997.
- [53] R. Luebbers, F. Hunsberger, K. Kunz, and R. Standler, "**A frequency Dependent Finite Difference Domain Formulation for Dispersive Material**".*IEEE Tran.Electromagn.Comput.*32, 222-227 (1990).
- [54] M. A. Alsunaidi and A. Al-Jabr, "**A General ADE-FDTD Algorithm for the Simulation of Dispersive Structures**"*IEEE Photonics Tech. Lett.*, vol. 21, pp. 817-819, June 2009.

- [55] Naqavi, A.; Miri, M.; Mehrany, K.; Khorasani, S. "**Extension of Unified Formulation for the FDTD Simulation of Nonlinear Dispersive Media**" *IEEE Photonics Tech. Lett.*, vol. 22, no. 16, August 15, 2010.
- [56] Teixeira, F. L., W. C. Chew, M. Straka, M. L. Oristaglio, and T. Wang, "**Finite-difference time-domain simulation of ground penetrating radar on dispersive, inhomogeneous, and conductive soils**" *IEEE Trans. Geos. and Remot. Sensing*, Vol. 36, No. 6, 1928-1937, Nov. 1998.
- [57] J. E. Hipp, "**Soil electromagnetic parameters as functions of frequency, soil density, and soil moisture**" *Proc. IEEE*, vol. 62, pp. 98–103, Jan. 1974.
- [58] F. J. Harris, "**On the use of windows for harmonic analysis with the discrete Fourier transform**" *Proc. IEEE*, vol. 66, pp. 51–83, Jan. 1978.
- [59] Case, T., and Waag, R., "**Flaw identification from time and frequency features of ultrasonic waveforms**" *IEEE Trans. Ultrason. Ferroelec. Freq. Contr.* Vol. 43, pp. 592-600, July 1996.



# Vita

- Salem Ali Al-Otaibi.
- Born in Dhahran.
- Received B.S.c degree in Electrical Engineering from KFUPM, Saudi Arabia in June 2008.
- Joined Saudi Aramco, Inspection Department, August 2008.
- Member of American Society for Non-Destructive Testing (ASNT).
- Certified Level III in three different NDT methods.
- Completed M.S.c degree requirements at KFUPM, Saudi Arabia in January 2012.
- E-mails : [otaisald@aramco.com](mailto:otaisald@aramco.com) , [salem.alotibi@gmail.com](mailto:salem.alotibi@gmail.com)